The following publication Jiang, X. and Chan, T.L. (2022), "Lagrangian particle tracking with new weighted fraction Monte Carlo method for studying the soot particle size distributions in premixed flames", International Journal of Numerical Methods for Heat & Fluid Flow, Vol. 32 No. 6, pp. 1961-1998 is published by Emerald and is available at https://dx.doi.org/10.1108/HFF-04-2021-0247

Lagrangian Particle Tracking with New Weighted Fraction Monte Carlo Method for Studying the Soot Particle Size Distributions in Premixed Flames

Xiao Jiang and Tat Leung Chan*
Department of Mechanical Engineering, The Hong Kong Polytechnic University, Hong Kong SAR, China

*Corresponding author
Tat Leung Chan can be contacted at: mmtlchan@polyu.edu.hk

Abstract

Purpose – The purpose of this paper is to study the soot formation and evolution by using this newly developed Lagrangian particle tracking with weighted fraction Monte Carlo (LPT-WFMC) method.

Design/methodology/approach – The weighted soot particles are used in this MC framework and is tracked using Lagrangian approach**.** A detailed soot model based on the LPT-WFMC method is used to study the soot formation and evolution in ethylene laminar premixed flames.

Findings– The LPT-WFMC method is validated by both experimental and numerical results of the direct simulation Monte Carlo (DSMC) and Multi-Monte Carlo (MMC) methods. Compared with DSMC and MMC methods, the stochastic error analysis shows this new LPT-WFMC method could further extend the particle size distributions (PSDs) and improve the accuracy for predicting soot particle size distributions at larger particle size regime.

Originality/value– Compared with conventional weighted particle schemes, the weight distributions in LPT-WFMC method are adjustable by adopting different fraction functions. As a result, the number of numerical soot particles in each size interval could be also adjustable. The stochastic error of PSDs in larger particle size regime can also be minimized by increasing the number of numerical soot particles at larger size interval.

Keywords Lagrangian particle tracking; weighted fraction Monte-Carlo method; detailed soot model; particle size distribution; stochastic error analysis

Paper type Research paper

1. Background

Combustion occurs in many different combustion systems, such as industrial or domestic burners and internal combustion engines. The combustion of hydrocarbon fuels is one of the important sources of energy. However, soot particles are always generated from the incomplete combustion of hydrocarbon fuels which can negatively affect our health and environment (Kumfer and Kennedy, 2009). Indeed, the soot formation and evolution are very complex phenomena due to the involvement of complex and concurrent physical and chemical processes such as gaseous/surface chemistry and aerosol dynamics (Wang, 2011). As a consequence, a deeper understanding of soot formation and evolution is essential for reducing serious air pollution and improving the cleaner combustion of fossil fuels.

In order to gain insight of the soot formation and evolution and obtain the detailed soot information, many soot models are proposed and classified into three categories (Kennedy, 1997): empirical soot models, semi-empirical soot models and detailed soot models, respectively. The empirical models determine the emission trend of soot particles by establishing a correlation for given experimental conditions (Micklow and Gong, 2002). Semi-empirical models combine empirical models with mathematical equations to describe the number density, volume and mass fraction of soot particles (Kazakov and Foster, 1998). Detailed soot models describe the full information about soot formation and evolution (i.e., the details gaseous and large polycyclic aromatic hydrocarbon (PAH) chemistry, the nucleation process, surface growth, PAH condensation, coagulation, and oxidation). However, the detailed soot models always require large computational resources (Wang *et al.*, 2016).

The evolution of soot particle size distributions (PSDs) can be modelled by a set of population balance equations (PBEs) (Marchisio and Fox, 2013) which are also called the general dynamic equations (GDEs) (Friedlander and Smoke, 2000). Since PBEs are series of the complex partial integral-differential equations, exact solutions of the PBEs rarely exist and are only available for a few fundamental cases (Smoluchowski, 1916). There are some numerical methods solving PBEs for soot particle dynamics which can be classified into three categories: sectional methods (SMs) (Prakash *et al.*, 2003, Gelbard *et al.*, 1980); methods of moments (MOM) (Frenklach, 2002, Yu *et al.*, 2008, Liu *et al.*, 2019b) and Monte Carlo (MC) methods (Zhou *et al.*, 2014, Zhao *et al.*, 2009, Liu *et al.*, 2019a, Liu and Chan, 2018a, Liu and Chan, 2019).

The MOM are computationally efficient methods, the evolution of moment equations are solved instead of resolving the whole PSDs (Mueller *et al.*, 2009). Due to the low computational cost of MOM, they are widely used to study soot formation in different fields such as diesel engines (Song and Zhong, 2008) and vehicle emissions (Chan *et al.*, 2010, Liu *et al.*, 2011). However, the details of soot PSDs are hardly to reconstruct from a finite set of moments. The SMs refer to discretize the PSDs to a number of sections with respect to the particle internal coordinate, then transform the PBEs to a

set of ordinary differential equations (ODEs) that describe the evolution of the sectional information including the total particle number and particle size in each section. A high computational accuracy can be achieved with sufficient number of sections, whereas they are computationally expensive with more than one internal coordinates (e.g. soot aggregates morphology) (Salenbauch *et al.*, 2015). Both MOM and SMs cannot provide the information about the trajectory and history of the individual soot particle, which are essential for studying soot formation and evolution (e.g., soot nucleation process is highly sensitive to the history of temperature and concentration of precursors). The MC methods are stochastic methods which are capable to solve the complex aerosol systems. Compared with MOM and SMs, MC methods have the advantage to incorporate several internal coordinates without causing much additional computational costs (Kraft, 2005, Menz and Kraft, 2013, Liu and Chan, 2017, Liu and Chan, 2018b). In addition, they are able to directly track the evolution of particle population so that the detailed PSDs can be obtained.

However, there are two disadvantages in the MC methods which are stochastic error and high computational costs (Xu *et al.*, 2015). In addition, only a finite number of numerical particles can be used, the uncertainty of PSDs function is inevitable. Especially at the tail of the particle size spectrum, only a few numbers of numerical particles are used which make the PSDs are poorly represented. In order to overcome such inherent limitations, the numerical particles with different numerical weights are adopted. The mass-flow algorithm (MFA) (Babovsky, 1999, Eibeck and Wagner, 2001), weighted flow algorithm (WFA) (DeVille *et al.*, 2011) and stochastic weighted particle method (SWPM) (Patterson *et al.*, 2011, Menz *et al.*, 2013) assign the numerical weight as the function of particle size/mass. In the abovementioned weighted schemes, more numerical particles can be assigned to the larger particle size regime, thus reducing the stochastic error for larger particle sizes. However, when the above weighted schemes are extended to the condensation/evaporation process, the total aerosol mass is also likely to vary in which the total number of numerical particles needs to be varied accordingly and constant-number scheme cannot be maintained. Although there are some remedies to maintain the constant-number scheme during the condensation/evaporation process, the algorithm will become more complicated (Debry *et al.*, 2003). The multi-Monte Carlo (MMC) method (Zhao *et al.*, 2009, Kotalczyk and Kruis, 2017) is another weighted scheme. In MMC method, the weight distribution is determined once the coagulation pairs are chosen. As a result, the weight distribution in MMC method cannot be adjustable. In the present study, the new weighted fraction Monte Carlo (WFMC) method is further derived based on the basic concept of MMC method. Compared with MMC method, the weight distribution in WFMC method can be adjusted. Hence, the assigned number of numerical particles in each size interval can be also adjustable. If more numerical particles are assigned to the larger particle size regime, the soot PSDs could be further extended and the stochastic error for larger particles could also be minimized.

The Lagrangian particle tracking (LPT) method can be used to obtain the individual soot particle trajectory and the history. In the LPT method, each numerical particle is tracked which represents a set of physical soot particles. The LPT method has been applied to study the transportation of soot particles in various conditions of flames (Katta *et al.*, 2005, Fuentes *et al.*, 2007, Tian *et al.*, 2020). However, there are only a few literatures on studying soot formation and evolution in Lagrangian point of view. Ong *et al.* (2018) firstly studied primary soot particle sizing by applying deterministic Lagrangian soot tracking method, however the soot particle coagulation process was not considered. This simplification cannot only reduce computational cost, but also induce deviation in their numerical simulation results since particle-particle interactions cannot be ignored in high soot concentration regime. Then Gallen *et al.* (2019) modelled and predicted soot formation by the semi-deterministic Lagrangian approach with the semi-empirical soot model. Coagulation process with the assumption of spherical soot particle is included in their semi-empirical model. The semi-empirical soot model based on the assumption of spherical soot particle can reduce complexity of their model, while the computational accuracy is also reduced. More recently, Dellinger *et al.* (2020) adopted the detailed gas-phase chemistry and soot model to simulate Lagrangian soot particle in one-dimensional laminar premixed ethylene-air flames. The assumption of spherical soot particle was used to all their studies but the soot morphology was not considered. Besides, the thermophoretic transport effect of soot particle was neglected in their model in which the computational accuracy was reduced when soot particle was undergone strong temperature gradients in the flame (Wu *et al.*, 2019). The present study adopts the Lagrangian soot particle as a dispersed solid phase, which can continuously track the trajectory of particles and obtain the information about interactions with gas species and other particles. In addition, the detailed soot model with soot morphology and thermophoretic effect is taken into consideration in order to gain the better insight into soot formation and evolution, which were not included in previous Lagrangian studies (Ong *et al.*, 2018, Gallen *et al.*, 2019, Dellinger *et al.*, 2020).

In the present study, the Lagrangian particle tracking coupled with weighted fraction Monte Carlo (LPT-WFMC) method is newly developed. The LPT-WFMC method is implemented in the OpenFOAM computational package (OpenCFD, 2019, Jasak *et al.*, 2007). The detailed chemical mechanisms of 101 species and 543 reactions with PAH chemistry up to pyrene (A4) is used as in (Appel *et al.*, 2000) because there have been some success in modelling soot formation in one-dimensional laminar premixed ethylene-air flames with ABF reaction mechanism (Yapp *et al.*, 2015, Hou *et al.*, 2019). In order to limit the computational time, only a subset of particles is considered and tracked, which is based on the concept of weighted particle by Zhao *et al.* (2009). In DSMC method, there are always insufficient number of numerical particles to represent larger particle sizes but are important for studying the soot PSDs due to their high contribution for high-order moment. As a result, this insufficient number of larger-sized numerical particles would lead to the narrower soot PSDs and also restricts the application of DSMC method. The concept of weighted particles is also introduced in

WFMC method, but with different implementations in coagulation process which the weight distributions can be varied and more numerical particles can be assigned for representing larger soot particles when comparing to DSMC method. On the other hand, the weight of soot particles has not been explicitly given as the function of particle size, which makes the present LPT-WFMC method more flexible in studying soot formation and evolution. Hence, the new LPT-WFMC method could extend the spectrum of soot PSDs and further reduce the stochastic error in larger particle size regime.

Compared with Eulerian methods and other MC methods, LPT-WFMC method is the newly developed method. The numerical simulations of LPT-WFMC method must be validated by comparison with the classical flame configurations. Although numerical simulations of two dimensional burner-stabilized stagnation (BSS) flames have already been conducted with some success in the work of Saggese *et al.* (2016), the discrepancies between the experimental measurements and numerical simulations may still be attributed to their adopted soot model and simulated flow fields. In addition, the flame condition C4 in Abid *et al.* (2008) was selected as benchmark flame condition to validate their developed numerical method in the recent work of Yang and Mueller (2019), the successful numerical validation is then obtained. For that reason, the present study is mainly focused on the numerical validation and also based on well-established one-dimensional burner stabilized flames at five different flame conditions in Abid *et al.* (2008). The paper is organized as follows: details on the implementation of the new LPT-WFMC method is firstly introduced. Then the numerical validation of the newly developed LPT-WFMC method in one-dimensional laminar premixed flames is conducted together with the stochastic error analysis. The sensitivity analysis of different model parameters on the soot PSDs is also studied. Finally, the major significant findings and conclusions are drawn.

2. Numerical method

2.1 Gas phase model

The governing equations of gas-phase combustion include the conservation of mass, momentum and energy, gas species mass fractions, which can be described as follows (Kuo, 2005):

$$\frac{\partial \rho}{\partial t} + \frac{\partial \rho u_i}{\partial x_i} = S_m \tag{2.1}$$

$$\frac{\partial \rho u_j}{\partial t} + \frac{\partial \rho u_i u_j}{\partial x_i} = -\frac{\partial P}{\partial x_j} + \frac{\partial \tau_{ij}}{\partial x_i} + S_j \tag{2.2}$$

$$\frac{\partial \rho Y_k}{\partial t} + \frac{\partial \rho u_i Y_k}{\partial x_i} = -\frac{\partial \rho Y_k V_{k,i}}{\partial x_i} + W_k \omega_k + S_k \tag{2.3}$$

$$\frac{\partial \rho E}{\partial t} + \frac{\partial \rho u_i E}{\partial x_i} = -\frac{\partial q_i}{\partial x_i} - \frac{\partial u_i P}{\partial x_i} + \frac{\partial u_j \tau_{ij}}{\partial x_i} + \omega_T + S_T \tag{2.4}$$

where ρ is the gas mixture density, x_i is the coordinate in i direction (i= 1, 2, 3), u_j is the velocity in j component, P and τ_{ij} are the pressure and the stress tensor, respectively, Y_k is the mass fraction of the kth gas species, E is the internal energy of gas mixture, $\dot{\omega}_T$ and $\dot{\omega}_k$ are the chemical source term of energy and kth gas species, respectively. S_m, S_j, S_k, S_T are the source terms from the interaction between gas phase and soot particles include the mass, momentum, kth species, and energy, respectively.

In the present study, the gas phase equations are solved by the opensource computational fluid dynamics (CFD) library OpenFOAM (OpenCFD, 2019, Jasak *et al.*, 2007). The governing equations are integrated with the finite volume method (FVM). The discretization schemes are second-order upwind and central difference for convection and diffusion terms, respectively. The pressure-velocity coupling is achieved by the pressure-implicit with splitting of operators (PISO) algorithm (Issa, 1986).

2.2 Soot model

In the present study, a soot particle is described as a fractal aggregate as joint surface-volume model (Blanquart and Pitsch, 2009) which consists of the number of primary particles, n_p with diameter, d_p. The total volume, V and total surface, S of a soot aggregate can be expressed as

$$V=\frac{\pi}{6}n_p d_p^3 \tag{2.5}$$

and

$$S=\pi n_p d_p^2 \tag{2.6}$$

The gyration diameter, d_g can be related to the primary particle diameter as described by Thajudeen *et al*. (2015) and Sorensen (2011):

$$n_p = k_f\left(\frac{d_g}{d_p}\right)^{D_f} \tag{2.7}$$

where k_f is the pre-fractal factor of 1.0 and D_f is the fractal dimension of the aggregates of 1.8 from Blanquart and Pitsch (2009). The effects of these parameters on PBM had been fully investigated by Yu *et al* (2017). In the present study, it is assumed that the diameters of mobility and collision are equal to each other which have been widely used in the previous modelling studies of laminar sooting flames (Blanquart and Pitsch, 2009, Mueller et al., 2009, Salenbauch et al., 2015, Yapp et al., 2015, Liu et al., 2019a, Kholghy and Kelesidis, 2021). The collision diameter, d_c of aggregates is determined from the Equation (2.8) as described by Yapp et al. (2015):

$$d_c = d_p n_p^{1/D_f} \tag{2.8}$$

Soot nucleation (Blanquart and Pitsch, 2009, Mueller *et al.*, 2009), surface reactions of hydrogen abstraction acetylene addition (HACA) (Frenklach and Wang, 1991), condensation of PAH on soot surface (Blanquart and Pitsch, 2009), oxidation by hydroxide (OH) and oxygen (O_2) (Kazakov *et al.*, 1995), and the particle coagulation are considered in the present study. However, the soot fragmentation in premixed ethylene flame is not considered in the present study after taking into account the negligible effect of oxidation-induced particle fragmentation under the present flame conditions as described in Saggese *et al*. (2015). For gas phase model, only pyrene consumption is considered when solving gas species equation for soot. The source term of species equation for pyrene is accounted by the consumption of soot nucleation and mass growth from pyrene. The details of these soot aerosol dynamic processes can be referred to (Wang, 2011).

2.2.1 Lagrangian formalism

In the Largrangian particle tracking model, each soot particle is tracked individually. The fluid characteristics (e.g., velocity, density etc.) on the soot particles are applied by linear interpolation on control volume (Jasak *et al.*, 2007)**.** The trajectories of the soot particles are evolved by:

$$\begin{cases} \dfrac{d\vec{x}_p}{dt} = \vec{u}_p \\ \dfrac{d\vec{u}_p}{dt} = f_{\text{drag}} + f_s \end{cases} \tag{2.9}$$

where f_{drag} is the particle velocity changed due to the drag force, and f_s represents the contributions from other forces but thermophoretic force is only considered in the present study. The drag force can be formulated by (Fan *et al.*, 1997):

$$f_{\text{drag}} = \frac{3}{4}\frac{\rho_f}{\rho_p d_p} C_D(\vec{u}_f - \vec{u}_p)\left|\vec{u}_f - \vec{u}_p\right| \tag{2.10}$$

where ρ_f and $\vec{u}_f$ are the density and velocity of surrounding fluid, respectively. The equation for drag coefficient, C_D, is written as (Zhu *et al.*, 2007):

$$C_D = \begin{cases} 24(1+0.15Re_p^{0.687})/Re_p, & Re_p < 1000 \\ 0.44, & Re_p \geq 1000 \end{cases} \tag{2.11}$$

where Re_p is the relative particle Reynolds number as:

$$Re_p = \frac{d_p\left|\vec{u}_f - \vec{u}_p\right|}{\nu} \tag{2.12}$$

The Stokes number, *St* is applied to characterize the inertia effect of soot particles in flow fields (Rigopoulos, 2010), which is defined as:

$$St = \tau_p / \tau_f \tag{2.13}$$

where $\tau_p=\rho_p d_p^2/(18\rho_f \nu_f)$ is the particle relaxation time and τ_f is a flow characteristic time. If Stokes number is small relative to unity ($St << 1$), the soot particle can be assumed to be the non-inertial particle. Then, the trajectories of soot particles are evolved by:

$$\frac{dx_{p,i}}{dt} = u_{f,i} + u_{T,i} \tag{2.14}$$

where x_p , u_f and u_T are the position coordinates, the fluid velocity and thermophoretic velocity at the location of numerical particle, p, respectively. The thermophoretic velocity can then be expressed as proposed by Waldmann (1961)

$$u_T = -\frac{3\nu}{4(1+\frac{\pi}{8}\alpha_m)}\frac{\nabla T}{T} \tag{2.15}$$

where α_m is the accommodation factor with a value of 0.9 (Allen and Raabe, 1982). The inertia effect of soot particles in flame is numerically discussed in Section 3.

2.2.2 Nucleation

Soot nucleation (inception) is still less understanding due to its complex nature. Many debates on soot nucleation mechanisms and PAH are now considered as most likely soot precursors (Wang, 2011, Frenklach and Wang, 1994). In the present study, the soot nucleation is assumed as dimerization of PAH due to collision and sticking of PAH species:

$$\text{PAH} + \text{PAH} \Rightarrow \text{dimer} \tag{2.16}$$

Pyrene (A4) is usually considered as important species for soot nucleation due to its high concentration in flame and thermodynamic stability (Appel *et al.*, 2000). The soot nucleation process in the present study is considered as pyrene dimerization (Freklach and Wang, 1994) since it has been widely used and validated in many research studies, for example, soot in plug flow reactors (Wen *et al*., 2005), laminar premixed flames (Yapp *et al*., 2015), and laminar diffusion flames (Selvaraj *et al*., 2016, Qiu *et al*., 2019, Hoerlle *et al*., 2020). The nucleation rate is then calculated according to kinetic theory as (Frenklach and Wang, 1994) with the self-sticking coefficient of 0.025 as used by Blanquart and Pitsch (2009) and the nuclei size is assumed to be 0.87 nm which is actually the size of single pyrene molecule (Tang *et al.*, 2017). The numerical weight of any new particle is calculated by the number of new nuclei or assigned numerical weight in order to control the number of numerical particles. Since the pyrene molecule is consumed during nucleation events**,** the pyrene consumption rate in nucleation is accounted as a source term in the species equation.

2.2.3 Surface reactions

The surface growth and oxidation through the H-abstraction and acetylene addition (HACA) mechanism were developed by Frenklach and Wang (1994) and the reactions are listed as

$$\begin{aligned} &C_{Soot}-H + H \leftrightarrow C_{Soot}\bullet + H_2 \\ &C_{Soot}-H + OH \leftrightarrow C_{Soot}\bullet + H_2O \\ &C_{Soot}\bullet + H \rightarrow C_{Soot}-H \\ &C_{Soot}\bullet + C_2H_2 \rightarrow C_{Soot}-H + H \\ &C_{Soot}\bullet + O_2 \rightarrow 2CO + \text{products} \\ &C_{Soot}-H + OH \rightarrow CO + \text{products} \end{aligned} \tag{2.17}$$

The increasing soot mass is dominated by HACA surface reactions (Veshkini and Dworkin, 2017). The reaction rate constants of surface growth and soot oxidation are calculated by the kinetic data in Appel *et al.* (2000). The fraction of surface activate sites (α) for surface reactions with gas species is also adopted as (Appel *et al.*, 2000):

$$\alpha = \tanh(a / \log \mu_1 + b) \tag{2.18}$$

where μ_1 is the first size moment of the soot particle distribution, and a and b are fitted parameters with the same values used in Appel el al (2000). For oxidation by OH, the reaction rate constant is calculated with the reaction probability of 0.13 as used in the model of Neoh *et al.* (1981).

2.2.4 Condensation

The collision of gas-phase PAH species on soot surface results in soot condensation process, the soot mass will increase during condensation. As in the model of Appel *et al.* (2000), pyrene-soot condensation is included in the present study. The condensation rate is depended on the collision frequency which could be calculated by the collision theory between pyrene molecules and soot particles (Park *et al.*, 2005, Kronholm and Howard, 2000). The pyrene-soot surface condensation efficiency is assumed to be 0.5 by Zhang *et al.* (2009) which describes the probability of sticking in each collision event. The pyrene consumption rate in condensation process is accounted as a source term in the species equation.

2.2.5 Coagulation

The coagulation process represents the collision of two soot particles of volumes v and u to form a new particle of volume $v + u$ which can be described by Smoluchowski equation (Smoluchowski, 1916)

$$\frac{\partial n(v,t)}{\partial t} = \frac{1}{2}\int_0^v \beta(u, v-u) n(u,t) n(v-u,t) du - \int_0^\infty \beta(v,u) n(v,t) n(u,t) du \tag{2.19}$$

where $\beta(u, v)$ is the collision kernel function which defines the collision rates for two particles with volumes, u and v. The collision kernel function depends on the Knudsen

number, Kn of the collision pairs. The Kn is described as the ratio of the mean free path to collision diameter. For Kn > 10, the free molecular regime coagulation kernel is used as:

$$\beta^{fm}(v,u) = 2.2\sqrt{\frac{\pi k_B T}{2m_{v,u}}}(d_c(v)+d_c(u))^2 \tag{2.20}$$

where $m_{v,u}$ is the reduced mass (Blanquart and Pitsch, 2009) and the multiplier 2.2 is the van der Waals enhancement factor (Frenklach and Wang, 1994). For Kn < 0.1, the continuum regime coagulation kernel is used as:

$$\beta^{c}(v,u) = \frac{2k_B T}{3\mu}(d_c(v)+d_c(u))(\frac{1}{d_c(v)}+\frac{1}{d_c(u)}) \tag{2.21}$$

where μ is the dynamic gas viscosity. For 0.1 < Kn < 10, the intermediate regime coagulation kernel is calculated by harmonic mean of $\beta^{fm}(v,u)$ and $\beta^{c}(v,u)$ as

$$\beta^{int}(v,u) = \frac{\beta^{fm}(v,u)\beta^{c}(v,u)}{\beta^{fm}(v,u)+\beta^{c}(v,u)} \tag{2.22}$$

2.2.6 Monte Carlo method

In the present study, the soot particle population balance is solved using a newly developed WFMC method which is based on the basic concept of MMC from Zhao *et al.* (2009). The operator splitting technique is adopted to deal with their different characteristic times to increase the computational efficiency. The Monte Carlo method is applied for stochastic process (i.e., coagulation process) and the deterministic integration method is applied for deterministic processes (i.e., nucleation, surface growth and condensation) with a second order Strang splitting scheme (Zhou *et al.*, 2014). Thus the smart bookkeeping method (Kruis *et al.*, 2000) can be used to evaluate the matrix of collision kernel to avoid a large time of recalculations, and save the computational resources in Monte Carlo simulation.

The detailed derivations of newly developed WFMC method can be found in the recent study of Jiang and Chan (2021), In here, only the brief description is presented. The main novelty of the WFMC method is about how to treat a coagulation event by introducing an additional fraction function, α. In MMC, the mean number of real coagulation events per real particle from i and j are considered as:

$$\Omega = \min(w_i, w_j) \tag{2.23}$$

In the present study, the less real coagulation event between two numerical particles is considered. Multiplying by a number between 0 and 1 which is so called the fraction function, α. The mean number of real coagulation events is then expressed as

$$\Omega' = \alpha_{ij}\min(w_i, w_j), \qquad \alpha_{ij} \le 1 \tag{2.24}$$

Thus, the new normalized coagulation kernel $\beta_{ij}^{'}$ considering the weights of particles, i and j is expressed as:

$$\beta_{ij}' = \frac{\max(w_i, w_j)}{\alpha_{ij}} \beta_{ij} \tag{2.25}$$

For the selected coagulation particle pair, i and j, with the numerical weight w_i and w_j. then the consequences of a coagulation event could be denoted as follows:

$$\text{if } w_i \neq w_j, \begin{cases} w_i'' = w_i - \alpha_{ij} \min(w_i, w_j); \quad v_i'' = v_i \\ w_j'' = w_j - \alpha_{ij} \min(w_i, w_j); \quad v_j'' = v_j \\ w_{\text{coag}}'' = \alpha_{ij} \min(w_i, w_j); \quad v_{\text{coag}}'' = v_i + v_j \end{cases} \tag{2.26}$$

$$\text{if } w_i = w_j, \begin{cases} w_i'' = w_i / 2; \quad v_i'' = v_i + v_j \\ w_j'' = w_j / 2; \quad v_j'' = v_i + v_j \end{cases} \tag{2.27}$$

where α_{ij} is the fraction of pysical particles between i, j which physical particles participate in coagulation events. w''' and v''' represent the new numerical weight and size of particles after the coagulation events. It should be noted that the number of numerical particles maintains constant only when $\alpha_{ij} \equiv 1$, then this WFMC method coincides with the MMC method at this condition. In order to maintain the number of numerical particles, one of particle i and j, should be removed randomly, and only one of particle i and j can be survived followed the probability as:

$$\begin{cases} P_i^{\text{birth}} = \dfrac{w_i - \alpha_{ij} \min(w_i, w_j)}{w_i - \alpha_{ij} \min(w_i, w_j) + [w_j - \alpha_{ij} \min(w_i, w_j)] \dfrac{v_j}{v_i}} \\ P_j^{\text{birth}} = \dfrac{w_j - \alpha_{ij} \min(w_i, w_j)}{w_j - \alpha_{ij} \min(w_i, w_j) + [w_i - \alpha_{ij} \min(w_i, w_j)] \dfrac{v_i}{v_j}} \end{cases} \tag{2.28}$$

Then the numerical weight of survived particles should be adjusted to:

$$\begin{cases} w_i''' = w_i - \alpha_{ij} \min(w_i, w_j) + [w_j - \alpha_{ij} \min(w_i, w_j)] \dfrac{v_j}{v_i} \\ w_j''' = w_j - \alpha_{ij} \min(w_i, w_j) + [w_i - \alpha_{ij} \min(w_i, w_j)] \dfrac{v_i}{v_j} \end{cases} \tag{2.29}$$

where the numerical weight of survived particles is adjusted to maintain the conservation of total particle number or volume.

The WFMC method (Jiang and Chan, 2021) is developed based on the basic concept of

MMC method (Zhao *et al*., 2009) but the implementation is similar to the weighted flow algorithm (WFA) (DeVille *et al*., 2011) which also removes the coagulated particle followed the probability in order to keep the conservation of total particle mass. It has already been proved that the methods with differential weight distribution can reduce the stochastic error for higher-order moments and PSDs in larger particle size regime (Zhou *et al*., 2020).

In Largrangian particle tracking model, for "non-coagulated" particle after a coagulation events, only the numerical weight in Equation (2.29) is assigned, and other properties (e.g., position, velocity, size etc.) remain unchanged. For "coagulated particle", their new properties are given as follows:

$$\begin{cases} w_{\text{coag}} = \alpha_{ij} \min(w_i, w_j) \\ v_{\text{coag}} = v_i + v_j \\ \vec{x}_{\text{coag}} = \dfrac{v_i}{v_i + v_j}\vec{x}_i + \dfrac{v_j}{v_i + v_j}\vec{x}_j \\ \vec{u}_{\text{coag}} = \dfrac{v_i}{v_i + v_j}\vec{u}_i + \dfrac{v_j}{v_i + v_j}\vec{u}_j \end{cases} \tag{2.30}$$

In the present study, the α_{ij} is always adopted in hyperbolic fraction function (HFF) type, and could be written as:

$$\alpha_{ij} = \frac{1}{1 + \min(v_i, v_j) / \max(v_i, v_j)} \tag{2.31}$$

A brief outline of the implementation of the LPT-WFMC method is given as follows:

Numerical Algorithm: LPT-WFMC method for the gas-soot phase	
Step 1.	Initialization. The boundary/initial conditions of both the gas and particle phases are assigned. For the gas phase, the initial thermal and flow fields (e.g., temperature, velocity, species mass fraction etc.) are characterized. For the particle phase, the soot particle properties (e.g., numerical weight, mass density, etc.) are characterized.
Step 2.	Choose a time-step, Δt for the gas phase flow.
Step 3.	Solving the gas flow fields. The governing equations of gas-phase combustion (i.e., conservation of mass, momentum, energy and species) are solved where the flow field properties (i.e., velocity, species molar fraction, temperature, etc.) are obtained.
Step 4.	Updating the spatial position and velocity of each particle. The motion of particles is governed by Equations (2.9) and (2.14), and thus the particle

field can be solved by the Lagrangian particle tracking (LPT) method.

Step 5. Choose a time-step, δt, for the soot aerosol dynamics.

Step 6. Start M (i.e., $M=\Delta t/\delta t$) Monte Carlo loops.

Step 7. Treatment of particle dynamic processes.

Step 8. The properties (e.g., numerical weight, size distribution, etc.) of simulated particles are updated.

Step 9. If the current MC loop number, R does not reach the predetermined MC loop number, M, then start a new MC loop. Otherwise, if R is equal to M, quit the Monte Carlo loop for calculating the soot aerosol dynamics.

Step 10. Advance time, t by using time step, Δt. If $t > t_{stop}$, the calculation is terminated, and the output results of particles and gas phase flow fields, else go to Step 2.

In order to obtain an accurate numerical simulation results with reasonable computational time, the number of numerical particles in each control volume should be within a certain range. Although the developed WFMC method could maintain constant number schemes during coagulation process, nucleation process and particles transportation from neighboring cells can introduce the fluctuation on number of numerical particles in the control volume. In MC simulation, resampling (Smith and Matsoukas, 1998) or resizing (Liffman, 1992) are always applied to maintain constant number of numerical particles. However, it has been proved that these methods will introduce stochastic error in numerical simulation (Zhou *et al.*, 2020). In the present study, the number of weighted numerical particles is controlled by the stochastic merging method in Kotalczyk and Kruis (2017) to reduce such resampling error.

3. Numerical validation of premixed laminar flames

In order to validate the newly developed LPT-WFMC method with the detailed soot model, the experimental results of one-dimensional premixed ethylene–oxygen–argon flames obtained from Abid et al. (2008) are adopted as a benchmark flame. The boundary conditions of the present numerical simulation used are the same as the experimental setup as listed in Table 1. The gas temperature and species profiles are studied by both reactingFOAM solver in OpenFOAM and Sandia 1-D PREMIX code (Kee *et al.*, 1985) which the Newton algorithm is used for gas phase steady-state solutions. OpenFOAM and PREMIX are both used the fixed mass-flux fraction for species boundary condition. The time step in OpenFOAM is fixed to 1 μs in order to satisfy the time scale for gas phase and aerosol dynamics. The simulated physical time is chosen large enough to reach a steady-state solution. A schematic diagram of all boundary conditions and meshes of the present study is shown in Figure 1.

Table 1 Test flame conditions (i.e., C_2H_4: 16.3%, O_2: 23.7%, Ar: 60%) (Abid *et al.*, 2008).

Flame cases	Cold gas velocity v_0 (cm/s)	Maximum flame temperature T_f (K)
C1	13	1898 ±50
C2	10	1805 ±50
C3	8	1736 ±50
C4	6.53	1710 ±50
C5	5.5	1660 ±50

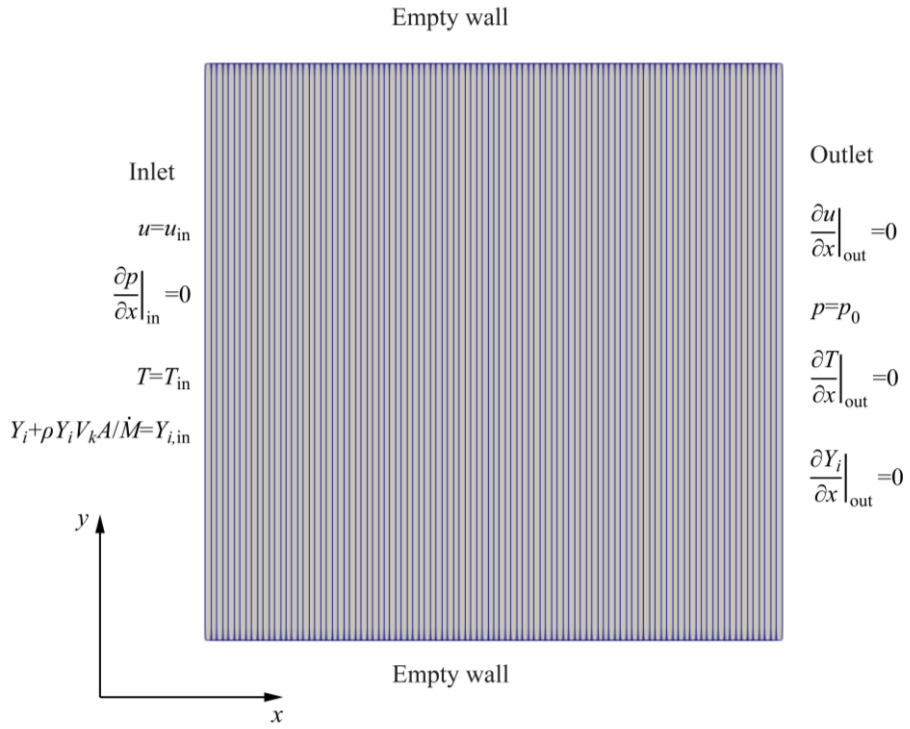

Figure 1 A schematic diagram of all boundary conditions and meshes.

The mesh grid contains a total of 1000 cells in the x-direction of 2 cm with a single cell in the y-direction because the present study is one-dimensional numerical simulation which is similar to many previous studies (Yapp *et al.*, 2015, Yang and Mueller, 2019, Hou *et al*., 2019, Liu *et al*., 2019a and Hou *et al*., 2020). The appropriate boundary conditions are deduced from the work of Kee *et al*. (1985) and Saggese *et al*. (2016). The Inlet boundary conditions consist of a set of prescribed velocity, burner temperature, mass flow rate of each species and the vanishing gradients for pressure. For the outlet boundary conditions, the pressure is given as the fixed value with the vanishing gradients for velocity, temperature and species.

3.1. Flame temperature and gas species concentration profiles

The typical flame temperature and gas species concentration profiles of flame C3 case are selected and presented in Figures 2 to 4. It is clear that the present numerical simulation results of temperature profiles agree well with both OpenFOAM and PREMIX. However, the numerical results obtained by the ABF model show slightly higher than the experimental results, especially for lower height above burner (HAB) flame region, the similar trends can also be found in other flame conditions (i.e., flame C1, C2, C4 and C5 cases). Such deviation is attributed to the heat losses of flame to the external environment which are difficult to be modeled (Kee *et al.*, 1985). Since soot nucleation process is sensitive to flame temperature, imposing the experimental flame temperature profile to the numerical simulation are very common (Hou *et al.*, 2019, Yang and Mueller, 2019). In the present study, the numerical simulations are both conducted by imposing the experimental flame temperature profile (Abid *et al.*, 2008) and by solving the energy equation in order to study the difference between these two approaches.

The gas species concentration profiles of flame C3 case are maintained nearly constant at post-flame region as shown in Figure 3. The present numerical simulation results by OpenFOAM (Jasak *et al.*, 2007) agree very well with the PREMIX (Kee *et al.*, 1985) and show the accuracy for small molecular species.

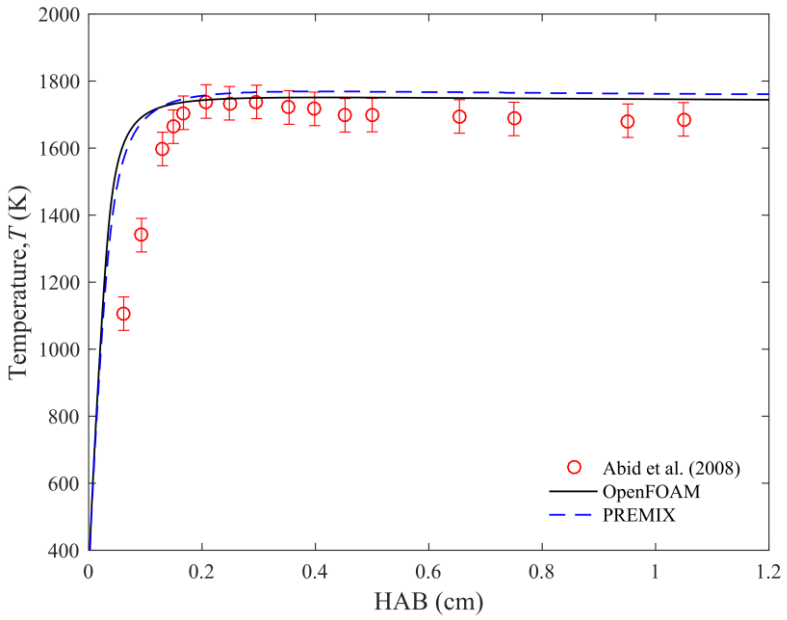

Figure 2 Comparison of experimental (Abid *et al.*, 2008) and numerical flame temperature profiles for different HABs at flame C3 case.

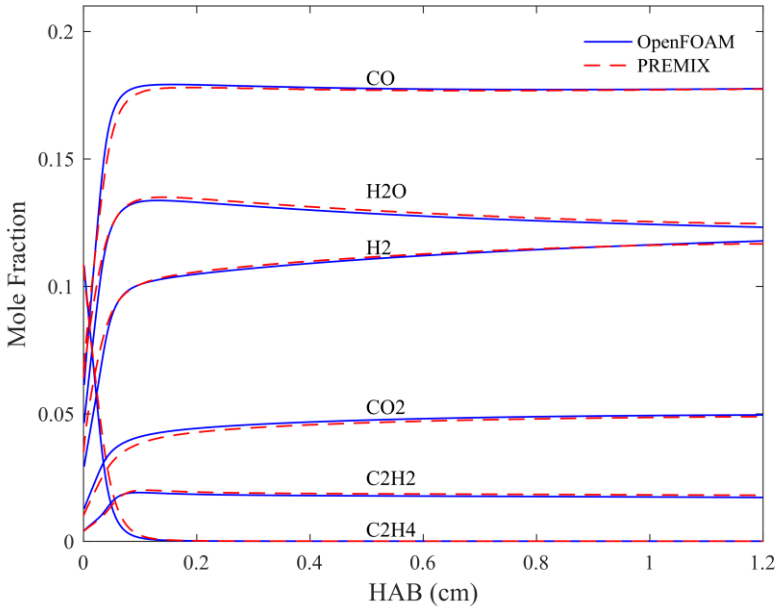

Figure 3 Comparison of the main gas species concentration profiles for different HABs by using OpenFOAM and PERMIX codes at flame C3 case.

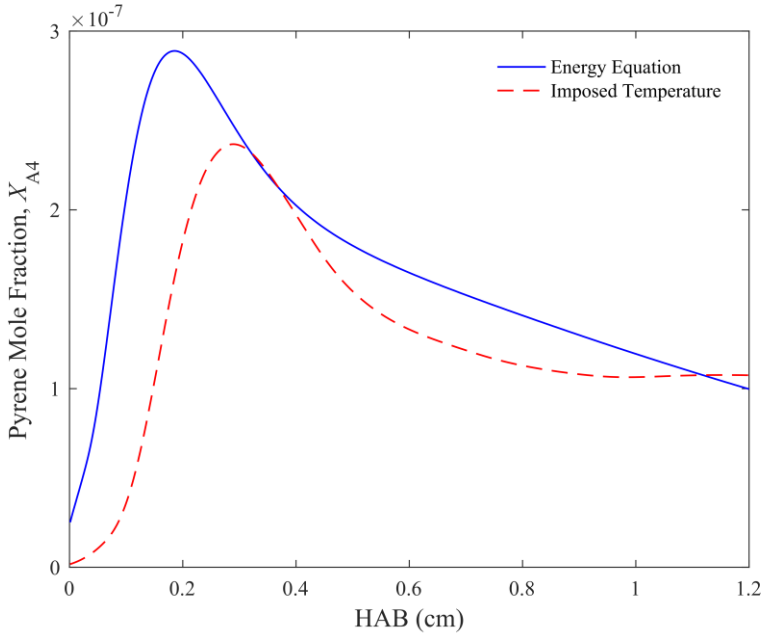

Figure 4 Comparison of the pyrene mole fraction profiles for different HABs by solving energy equation and imposing experimental flame temperature profiles at flame C3 case.

Figures 4 shows that the pyrene concentration increases in lower HAB, and then decreases at higher HAB. Such a trend is attributed to the competition between the inception of pyrene by the growth of PAH and the consumption of pyrene by the soot nucleation and condensation processes. In addition, the peak of pyrene mole fraction

profiles by imposing the experimental flame temperature profile is lower when compared with that by solving the energy equation. Different flame temperature profiles result in different pyrene mole fraction profiles which show the flame temperature effects on the soot precursors.

3.2 Evaluation of the algorithm

3.2.1 Lagrangian particle tracking

Figures 5 shows the average Lagrangian soot particle velocity profiles of flame C3 case for HABs from 0–0.12cm. The average particle velocity in each cell (The mesh grid contains a total of 1000 cells which are enough to resolve the flow fields in the present study) is defined as:

$$\bar{u}_i = \left. \frac{\sum_{j=1}^{N_i} u_{p,j} w_j}{\sum_{j=1}^{N_i} w_j} \right|_{x_{p,j} \in \text{cell } i} \tag{3.1}$$

where $\bar{u}_i$ is the average soot particle velocity in each cell i, $u_{p,j}$ is the velocity of jth particle in each cell i, and w_j is the numerical weight of j particle. It is clear that there is distinctive difference between the average soot particle velocity profiles with or without thermophoretic effect at lower HAB. For higher HAB, such thermophoretic effect is neglegible. This can be explained by considering the flame temperature profile in Figure 2. For lower HAB, the temperature gradient is large, which leads to a significant thermophoretic effect. For higher HAB, the temperature remains nearly constant, so the thermophoretic effect is minor. Compared with the average particle velocity profiles with or without inertial effect, the results are almost the same. This is attribute to the very low Stokes numbers ($St << 1$) of soot particles at the present flame conditions. It implies that the inertial effect of soot particles is neglegible. Therefore, the soot particles are assumed to be the non-inertial particles and the Lagrangian particle trajectories are evolved according to Equation (2.10).

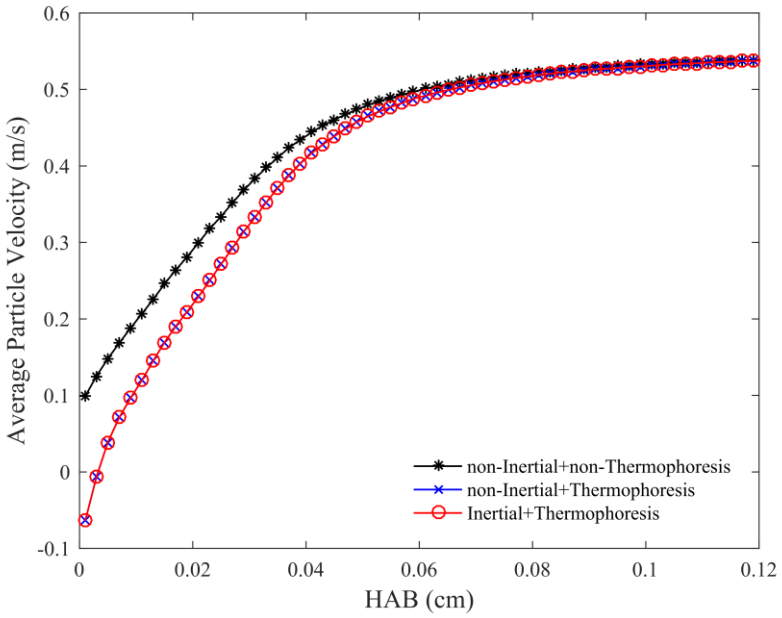

Figure 5 Comparison of the average particle velocity profiles with both inertial and thermophoretic effects for different HABs at flame C3 case.

3.2.2 Stochastic error analysis of the algorithm

Figure 6 shows the comparison of PSDs of flame C3 case by using different Monte Carlo methods (i.e., DSMC, MMC and WFMC methods) at HAB= 0.85 cm. All the numerical simulations using the same number of numerical particles with enough repetitions to obtain the average statistics converge results, (i.e., 500 of numerical particles with 200 independent repetitions). The results of normalized number density of soot particles are shown in Figure 6, which is given as

$$n(D_p) = \frac{1}{N}\frac{dN}{d\log D_p} \tag{3.2}$$

where D_p is the particle mobility diameter and N is total soot number density.

An excellent agreemnt is clearly observed among DSMC, MMC and WFMC methods for flame C3 case which is able to validate the present newly developed WFMC method as shwon in Figure 6. Besides, both the WFMC and MMC methods show the longer PSDs when compared with DSMC method but the WFMC method shows the longest PSDs among the other two MC methods. It is because WFMC method can change the numerical weight distributions of each particle size. In general, there are always insufficient number of numerical particles to represent larger particles due to their low soot number concentration. In WFMC method, the larger-sized numerical particles are assigned with much smaller numerical weights as shown on the left hand side of Figure 7. As a result, WFMC method always adopts more number of numerical particles to represent larger particles (but less to represent smaller particles) as shown on the right hand side of Figure 7 (where the C is the number of numerical particles).

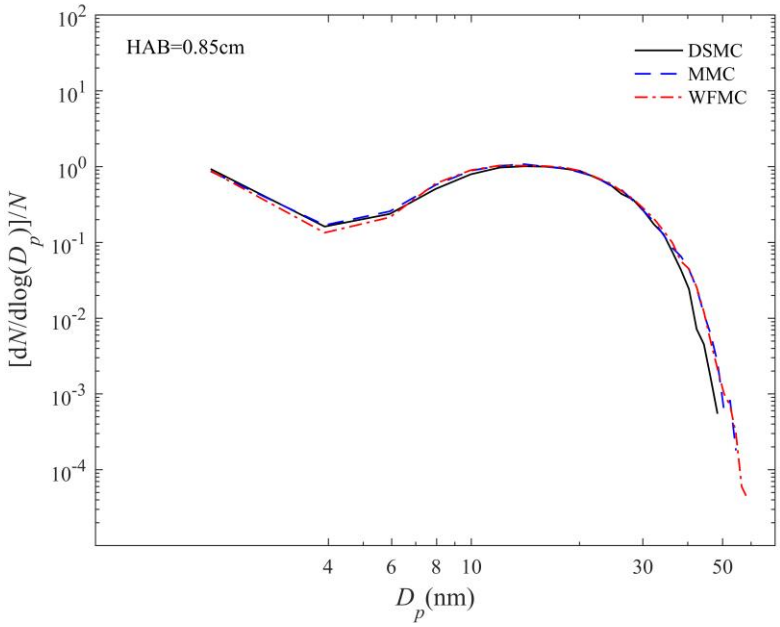

Figure 6 Comparison of the average particle size distributions at HAB = 0.85 cm by using DSMC, MMC and WFMC methods for flame C3 case.

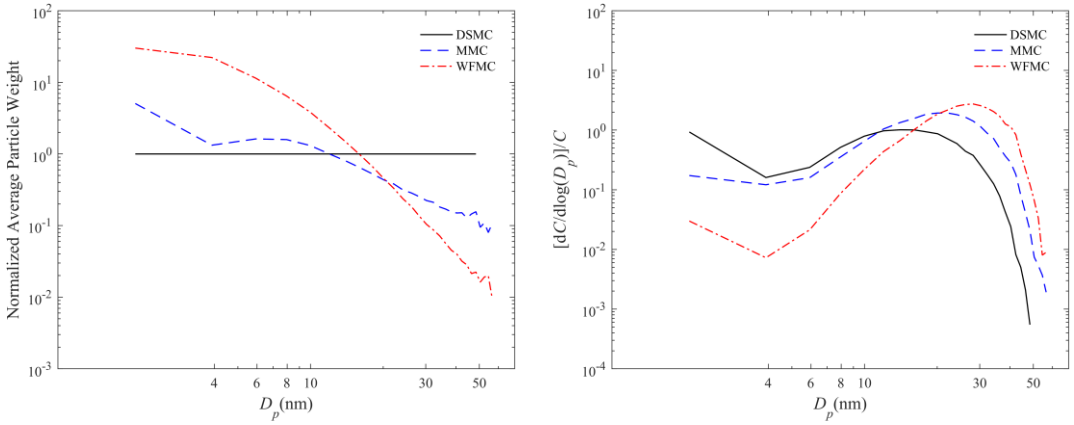

Figure 7 Comparison of (a) normalized average numerical weight distributions and (b) numerical particle size distributions by using DSMC, MMC and WFMC methods for flame C3 case.

The variance of PSDs is adopted to quantitively analyse the statistical uncertainty of different MC methods which is defined as:

$$\sigma^2(D_p) = \frac{1}{N_{\text{rep}} - 1} \sum_{i=1}^{N_{\text{rep}}} (n_i(D_p) - \overline{n(D_p)})^2 \tag{3.2}$$

where $n_i(D_p)$ denotes the ith repetition of the normalized soot number density, and $\overline{n(D_p)}$ denotes its sample mean as:

$$\overline{n(D_p)} = \frac{1}{N_{\text{rep}}} \sum_{i=1}^{N_{\text{rep}}} n_i(D_p) \tag{3.2}$$

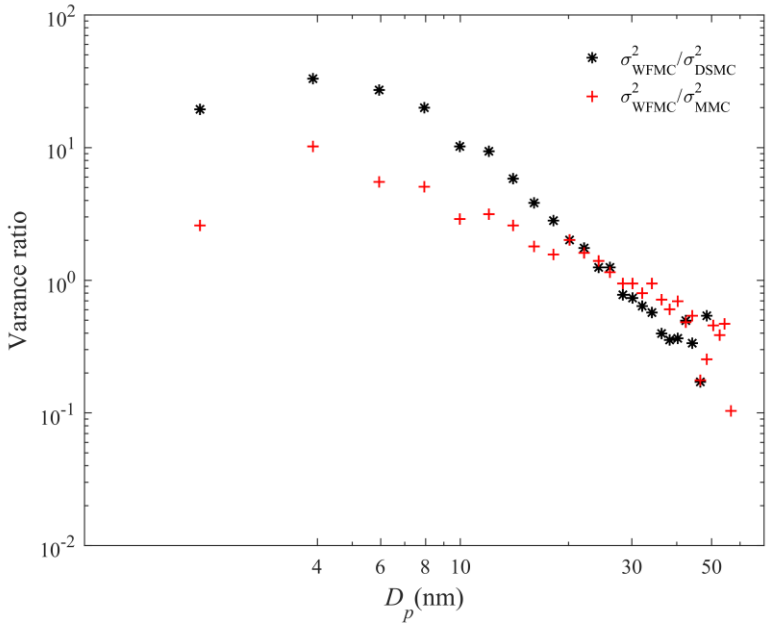

Figure 8 Comparison of the variance ratio by using DSMC, MMC and WFMC methods for flame C3 case.

Figure 8 shows the variance ratios of different Monte Carlo methods (i.e., DSMC, MMC and WFMC methods), which are denoted as σ^2_{DSMC}, σ^2_{MMC}, and σ^2_{WFMC}, respectively. As particle size increasing, the variance ratio between WFMC to DSMC, and WFMC to MMC both shows nearly linear trend of decreasing in the logarithm coordinate (except the first point at around 2 nm). It implies that when comparing with DSMC and MMC methods, there are larger variance in WFMC method for smaller particle size regime but the smaller variance in larger particle size regime. This analysis supports the capability of WFMC method to improve the accuracy of soot PSDs for larger particle size regime with less accuracy trade-off in smaller particle size regime. Since larger particle size regime has higher contribution for high-order moment but always is poorly represented, it is more important to improve the accuracy of soot PSDs for larger particle size regime. Besides, the reason for that the first point does not follow the linear trend of decreasing due to the nucleation is dominant process at the samllest size regime. The nucleation is implemented as deterministic integration as decribed in Section 2.2.6, thus different trends on statistical uncertainity are shown. Based on the error analysis, the WFMC method shows a great capacity for accurate prediction on the

larger particle size and it is also able to further extend the PSDs. Hence, LPT-WFMC method is used for making comparisons with soot experimental measurements in Section 3.3.

3.2.3 Remark on the computational cost

As a guideline for comparison to Lagrangian particle tracking with different MC methods, the Lagrangian solver contributes around 41%, 34% and 40% to the total computational time by using DSMC, MMC and WFMC methods, respectively in the present study. The total 60,000 numerical particles are used and 102 transport equations are solved for the gas-phase. The reason for a slightly higher computational time by around 6% for WFMC method than that of MMC method is because of the higher computational cost in coagulation events which could be attributed to two factors. On the one hand, WFMC method must deal with a more complex coagulation kernel when compared with the MMC method (i.e., the kernel function is $\max(w_i,w_j)\beta_{ij}/\alpha_{ij}$ in the WFMC method but is $\max(w_i,w_j)\beta_{ij}$ in the MMC method, as referred to the Equation (2.25)). Hence, a longer computational time is required to calculate the coagulation kernel in the WFMC method. On the other hand, the coagulation kernel function in the WFM method is always larger than that in the MMC method. The higher total coagulation rate, C_0, leads to more coagulation events in given time interval and higher computational time consumption.

3.3 Comparison with soot experimental measurements

3.3.1 Soot volume fraction/number density

Figures 9 and 10 show the total number density and volume fraction of soot particles by the experimental results of flame C1−C5 cases obtained from Abid *et al*. (2008) and the present numerical simulation results with the newly developed LPT-WFMC method. As mentioned clearly in Abid *et al.* (2008), the particle detection limit of their scanning mobility particle sizer (SMPS) was 2.5 nm, only for particle sizes larger than 2.5 nm were measured. Therefore, for comparison with the present numerical simulation and experimental (Abid *et al.*, 2008) results, the particles size smaller than 2.5 nm are also removed from the present numerical simulation results which are handled similar to the previous study of the same premixed flame in Salenbauch *et al.* (2015).

In Figure 9 show similar increasing and decreasing trends in both the numerical simulation and experimental results. The nucleation process dominates at lower HAB and causes a rapid increase in the total soot number density. But for higher HAB, the coagulation process becomes more important. The competition between nucleation and coagulation process causes a decrease in total soot number density at higher HAB. Compared with the results by solving the energy equation, the imposing experimental flame temperature profiles totally shift the results to the right, which show the effects of flame temperature profiles on total number density profiles of soot particles.

Compared with the experimental results, the overestimation of numerical results for total number density of soot particles can be especially observed for lower HAB**.** The similar large overestimation for total number density of soot particles also can be found in previous study of numerical simulation results (Yang and Mueller, 2019) with both sectional method and method of moments. The overprediction on the total number density of soot particles indicates that the present numerical simulation results of current soot model overpredict the number of smaller particles when compared with the experimental results, which may be attributed to the higher soot nucleation rate used.

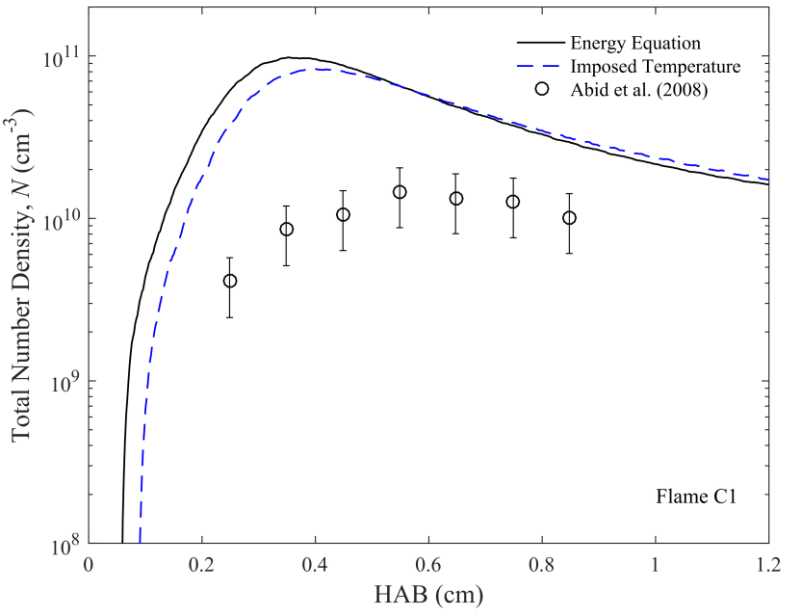

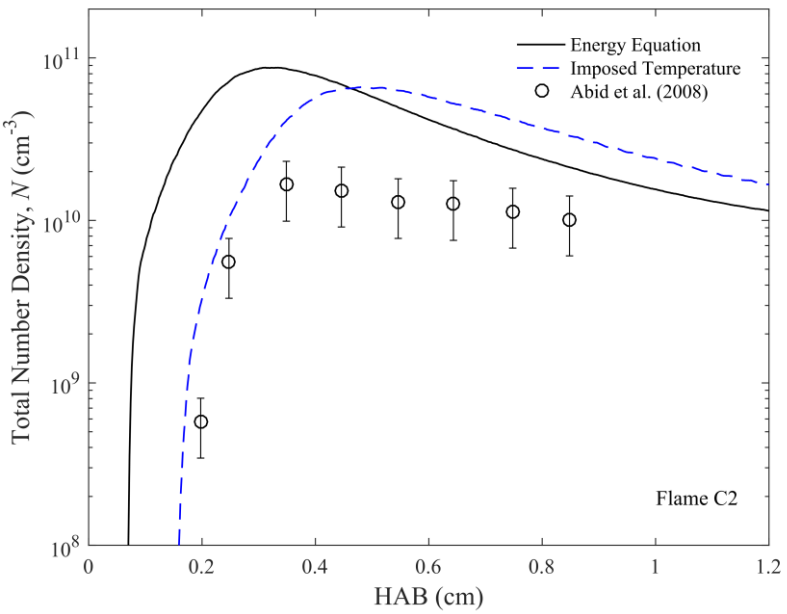

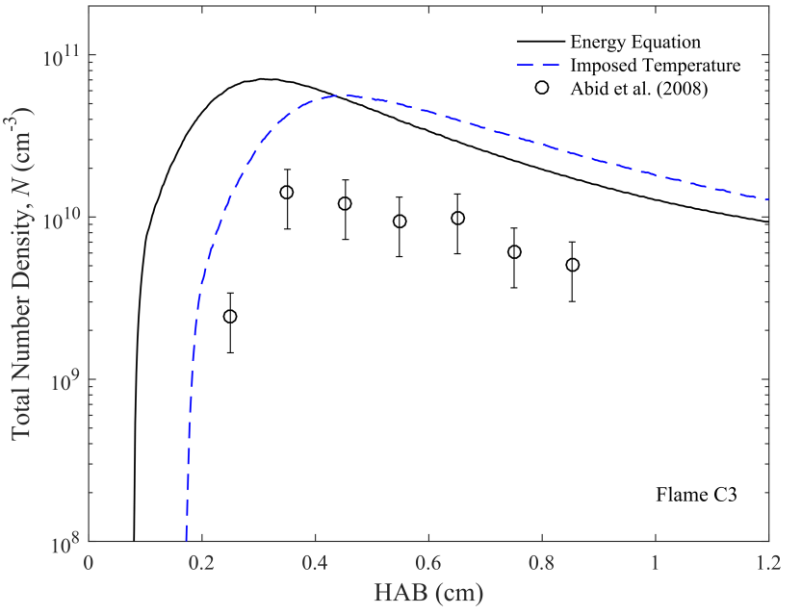
Energy Equation
Imposed Temperature
Abid et al. (2008)
Flame C3
Total Number Density, N (cm-3)
HAB (cm)
10^11
10^10
10^9
10^8
0
0.2
0.4
0.6
0.8
1
1.2

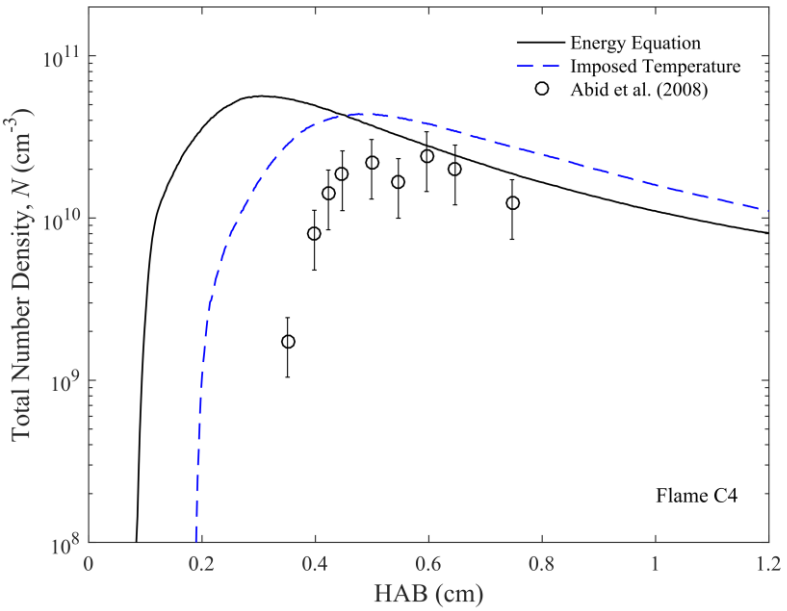
Energy Equation
Imposed Temperature
Abid et al. (2008)
Flame C4
Total Number Density, N (cm-3)
HAB (cm)
10^11
10^10
10^9
10^8
0
0.2
0.4
0.6
0.8
1
1.2

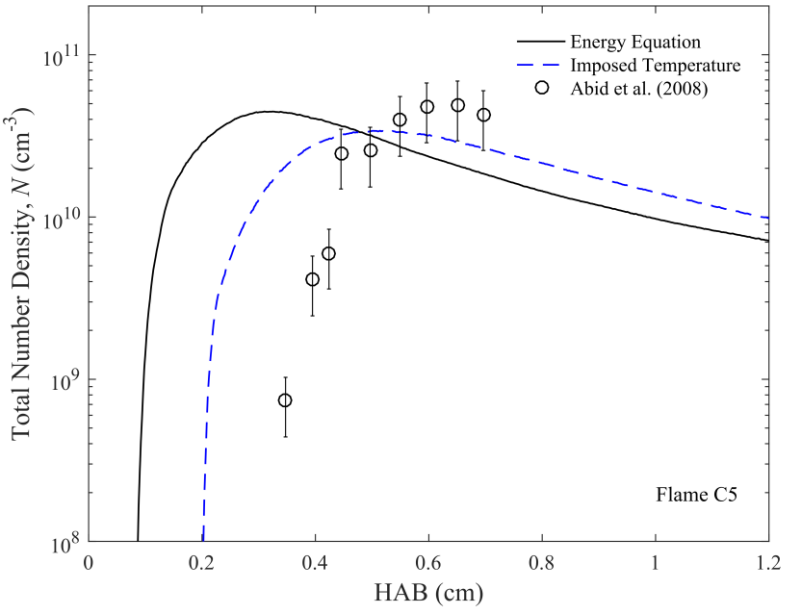

Figure 9 Comparison of total number density profiles of soot particles between the present numerical simulation and experimental (Abid *et al.*, 2008) results for different HABs and flame condition cases.

In Figure 10, the numerical simulation results of soot volume fraction of flame C1 case are close each other by solving the energy equation and imposing the experimental flame temperature profile. This is due to the flame temperature profile in flame C1 case by solving the energy equation are nearly the same as that of experimental results. For flame C2–C5 cases, the soot volume fractions of the experimental results (Abid *et al.*, 2008) are at the approximate range between the numerical simulation results by solving the energy equation and by imposing the experimental flame temperature profiles.

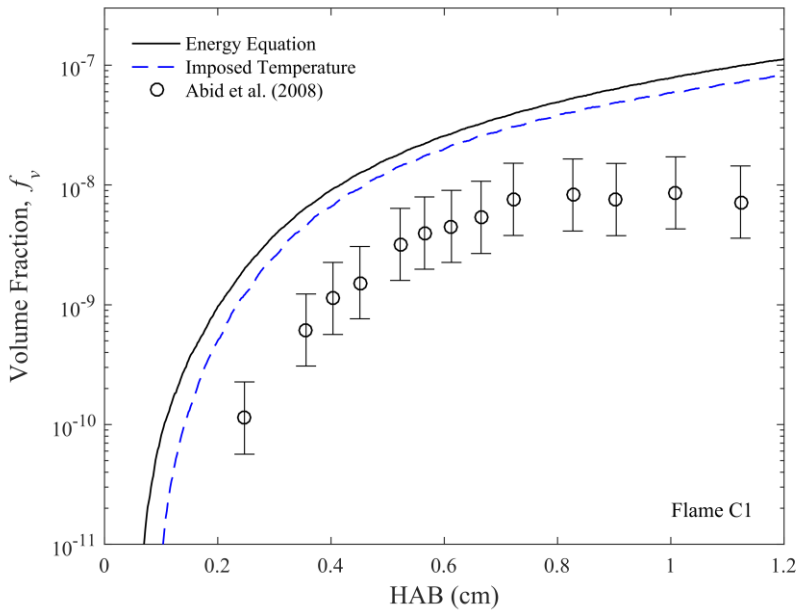

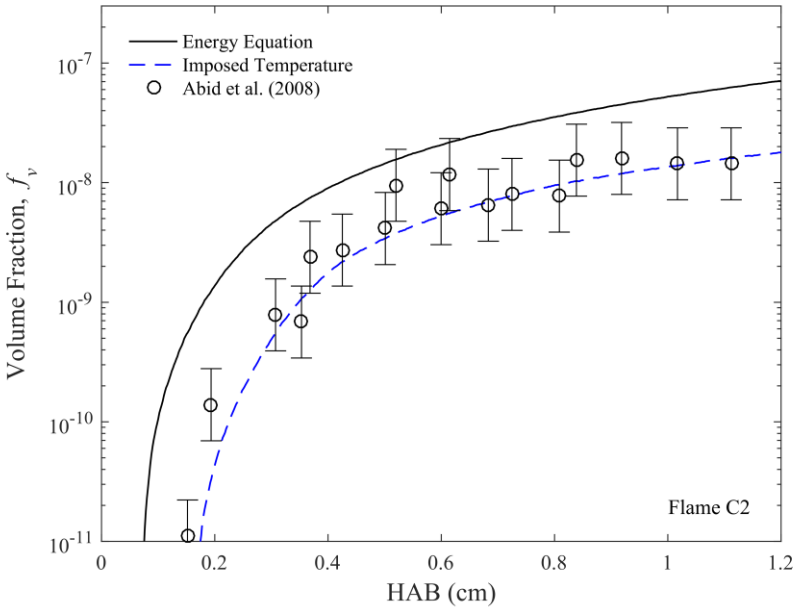
Energy Equation
Imposed Temperature
Abid et al. (2008)
Volume Fraction, f_v
HAB (cm)
Flame C2
10^{-7}
10^{-8}
10^{-9}
10^{-10}
10^{-11}
0
0.2
0.4
0.6
0.8
1
1.2

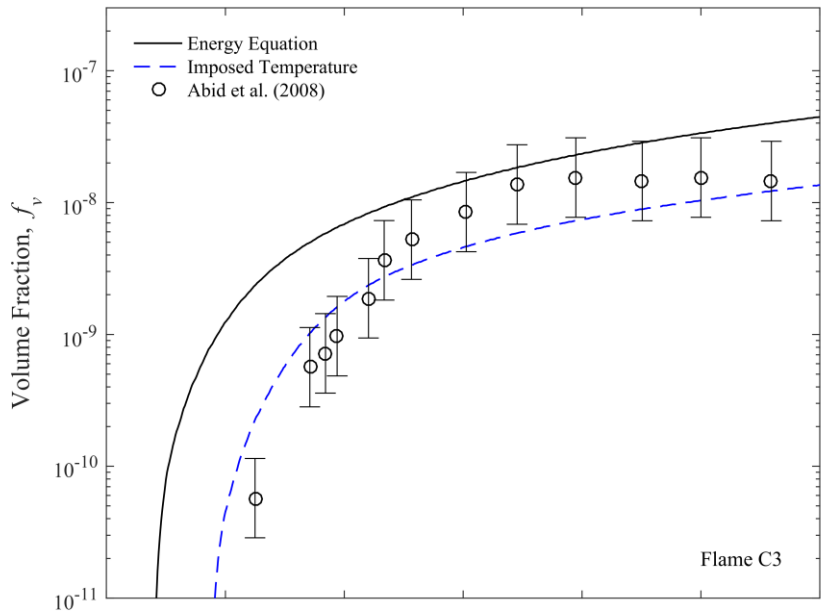
Energy Equation
Imposed Temperature
Abid et al. (2008)
Volume Fraction, f_v
Flame C3
10^{-7}
10^{-8}
10^{-9}
10^{-10}
10^{-11}

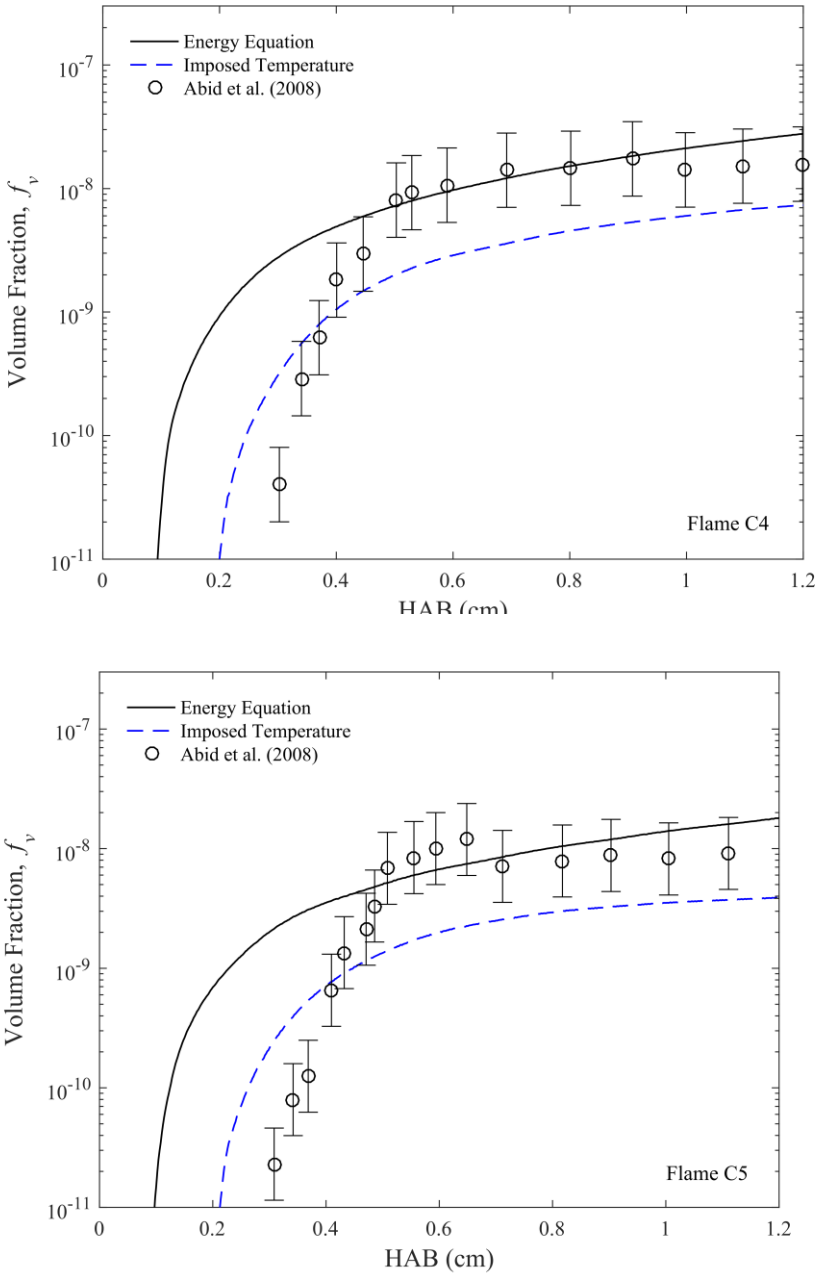

Figure 10 Comparison of soot volume fraction profiles between the present numerical simulation and experimental (Abid *et al.*, 2008) results for different HABs and flame condition cases.

3.3.2 Soot particle size distributions

The results for PSDs for different heights above the burner (HABs) are shown in Figures 11 to 15. By imposing the experimental flame temperature profiles, the results are totally shifted to the left as compared to the results of solving the energy equation. As shown in Figure 4, imposing of the experimental flame temperature profile which leads to lower the peak of pyrene concentration, thus reduce the nucleation rate as well as the condensation rate, and shifts the PSDs to smaller particle size regime.

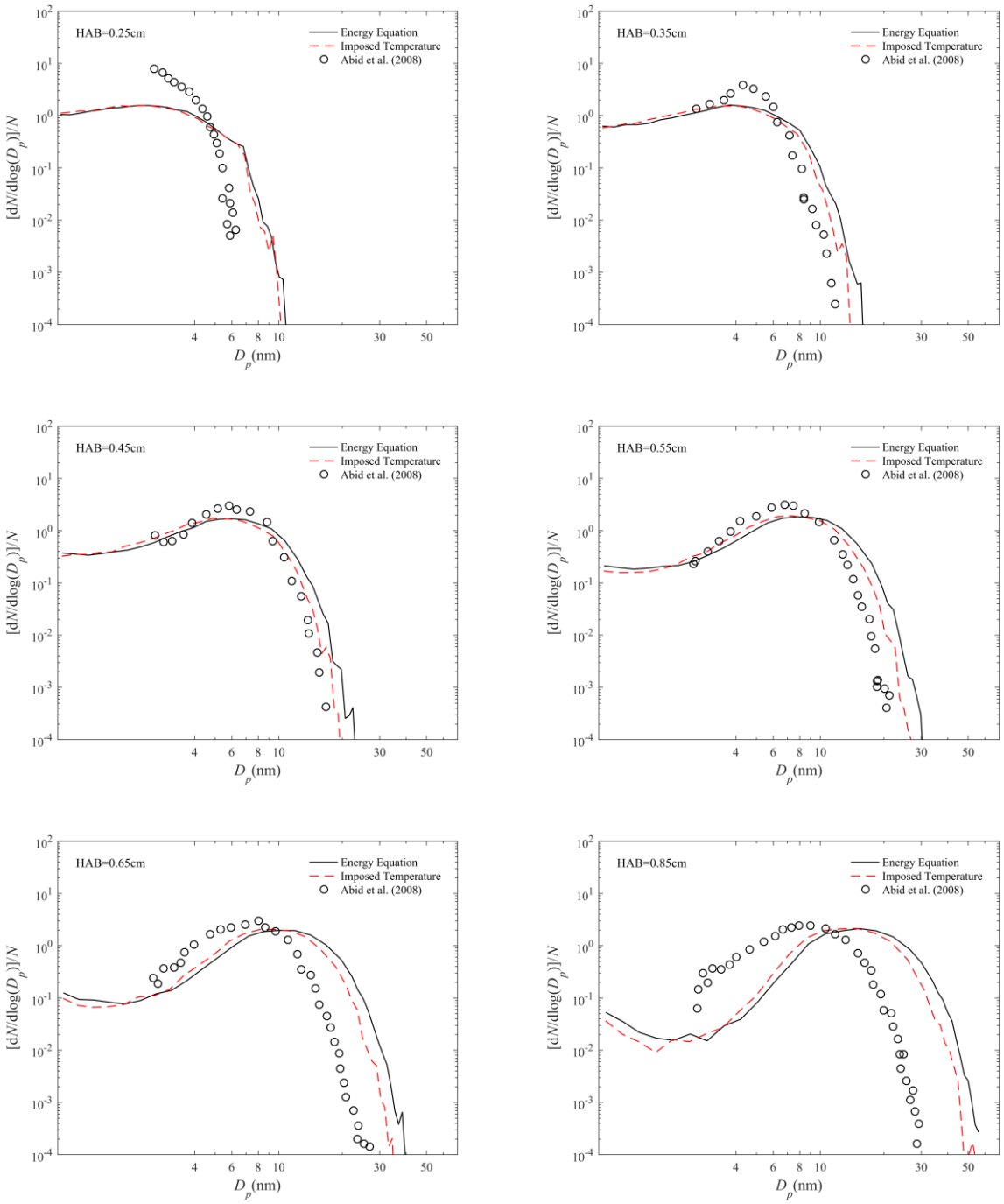

Figure 11 Comparison of particle size distributions of flame C1case between the present numerical simulation and experimental (Abid *et al.*, 2008) results for different HABs.

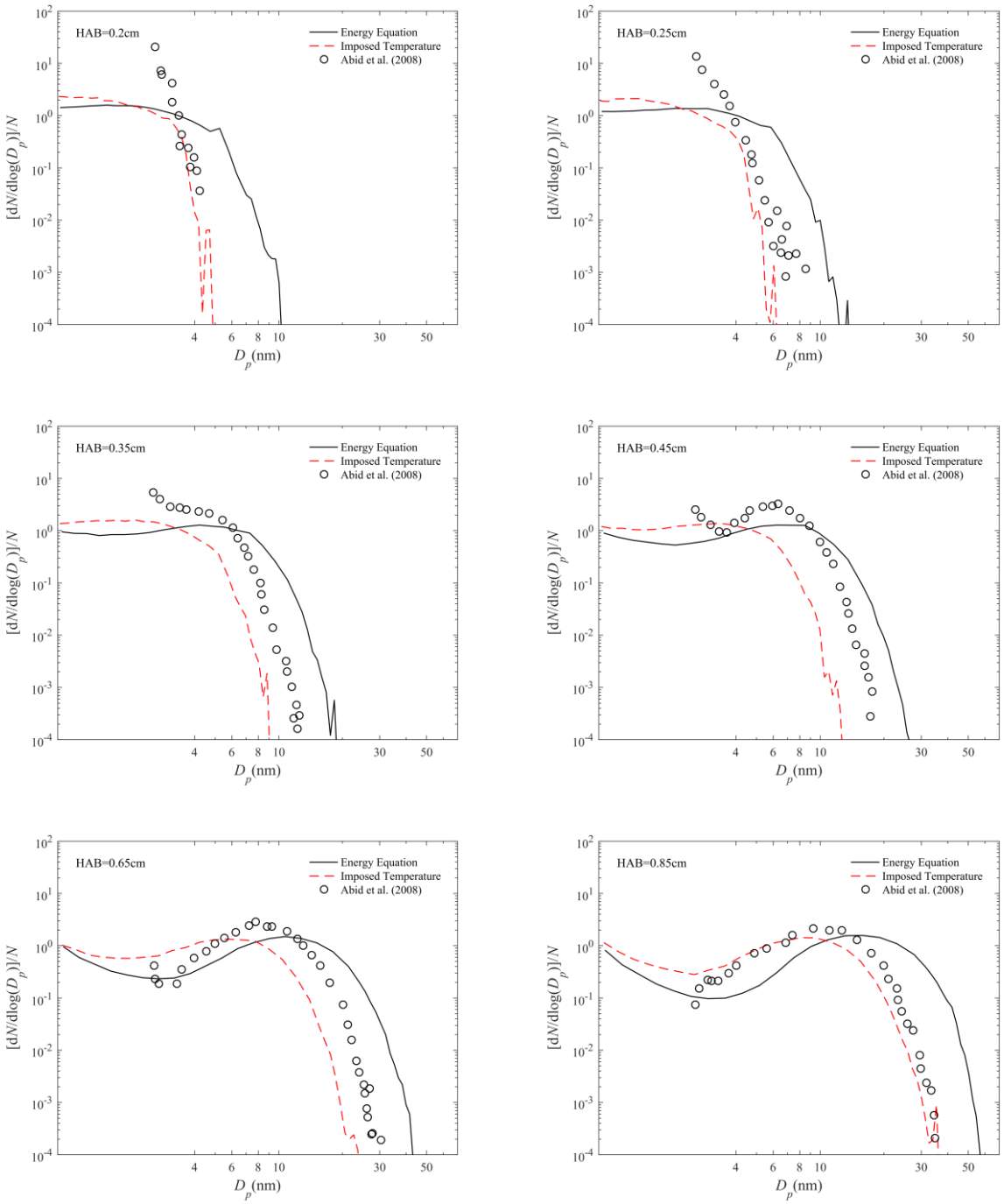

Figure 12 Comparison of particle size distributions of flame C2 case between the present numerical simulation and experimental (Abid *et al.*, 2008) results for different HABs.

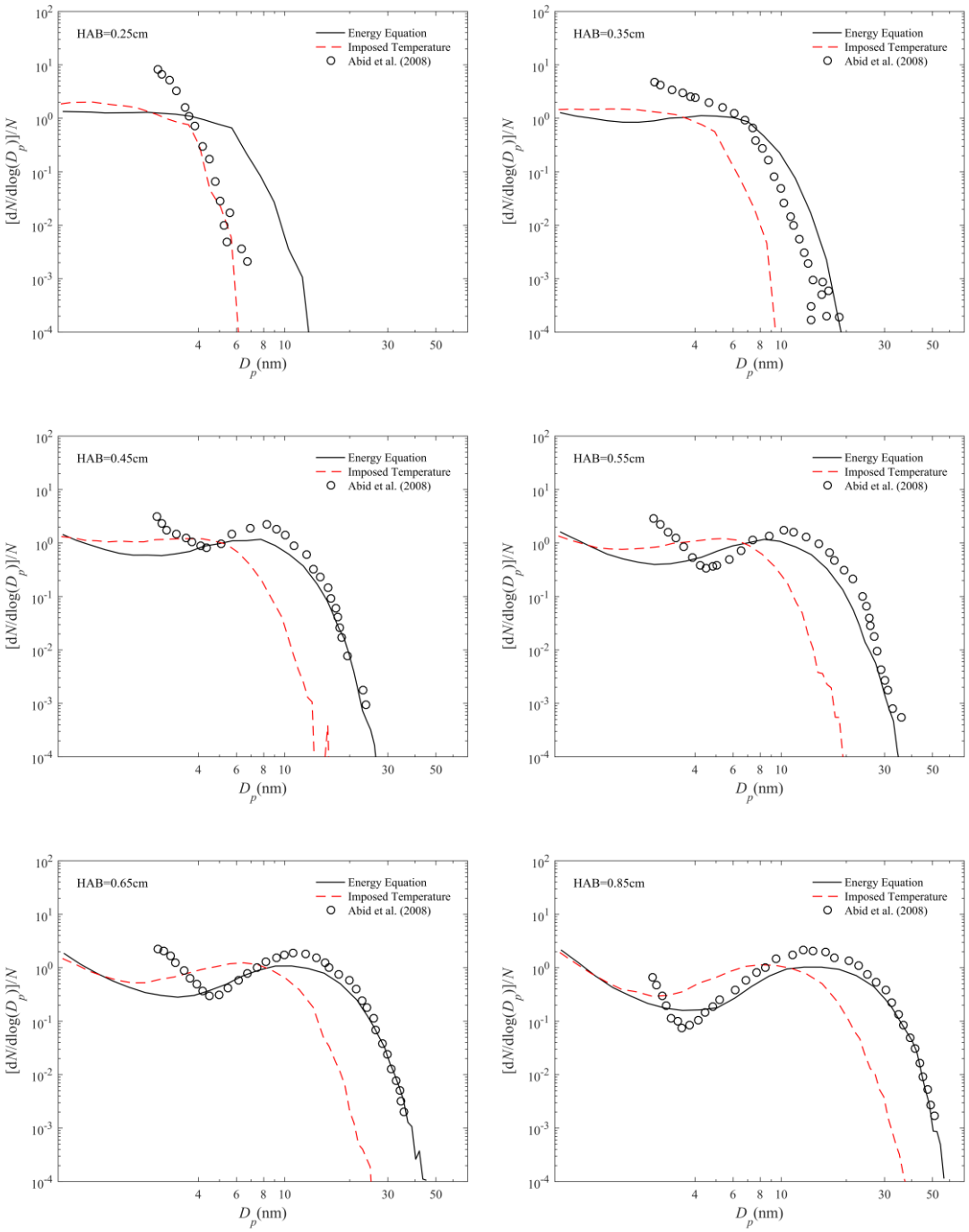

Figure 13 Comparison of particle size distributions of flame C3 case between the present numerical simulation and experimental (Abid *et al.*, 2008) results for different HABs.

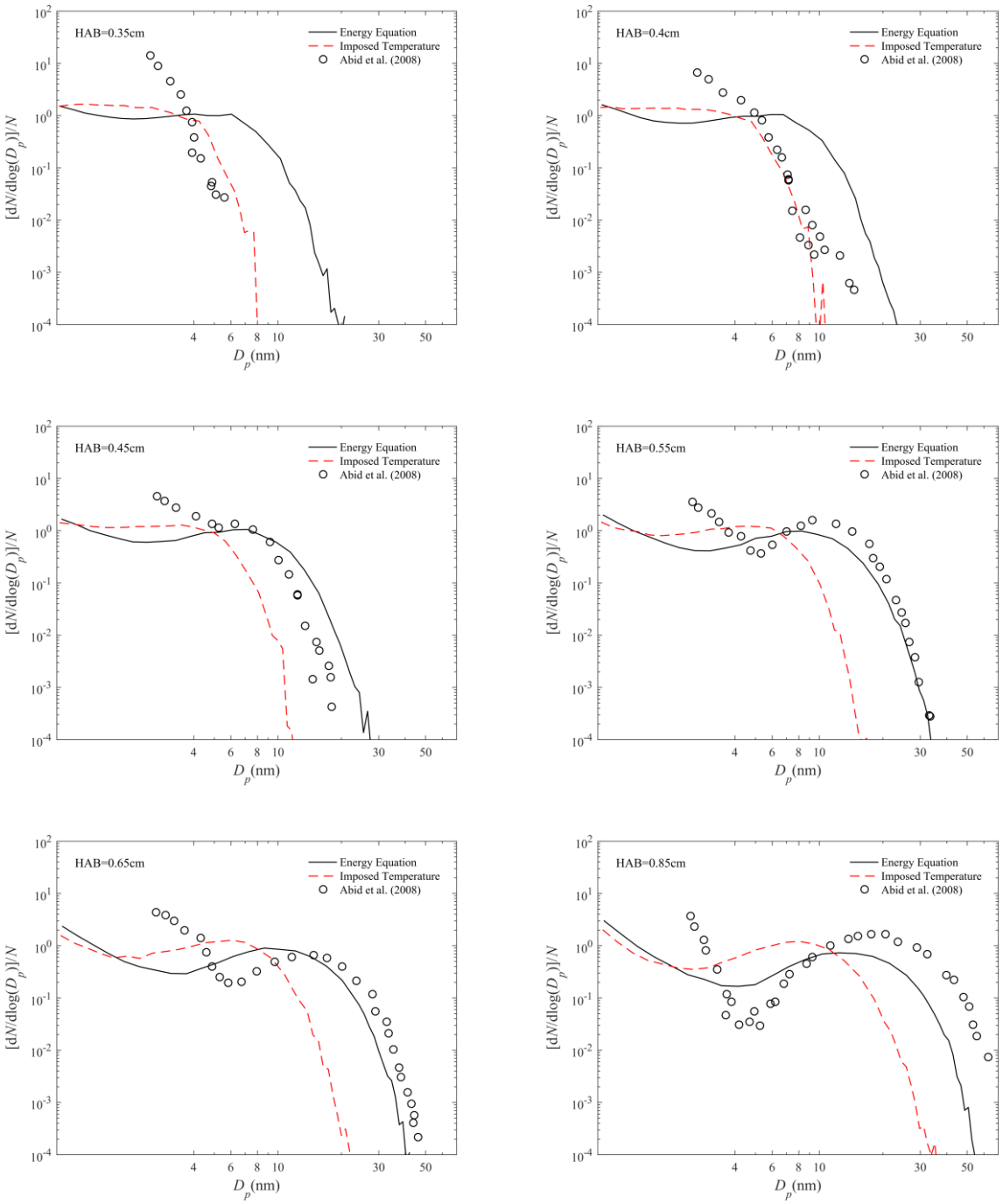

Figure 14 Comparison of particle size distributions of flame C4 case between the present numerical simulation and experimental (Abid *et al.*, 2008) results for different HABs.

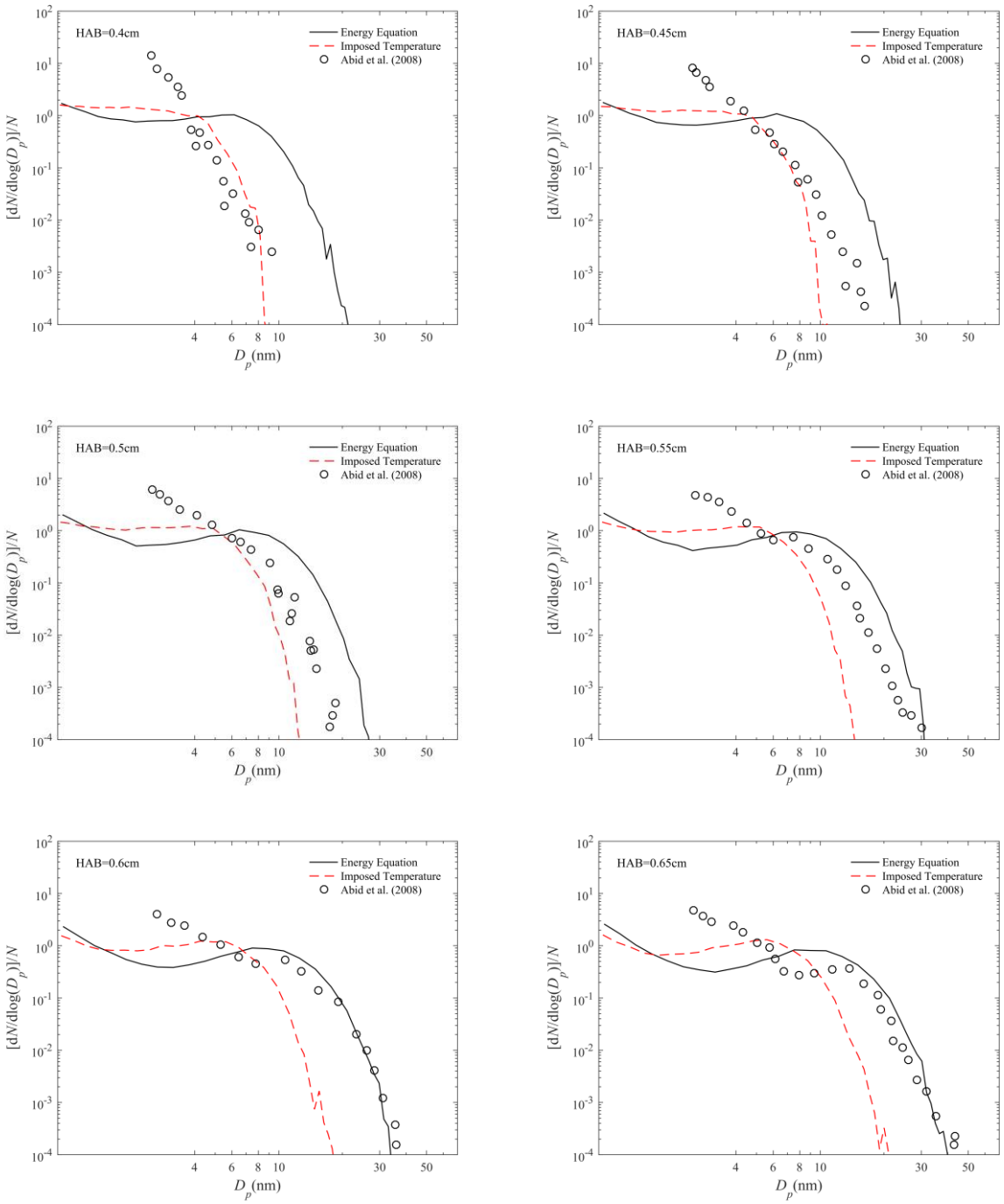

Figure 15 Comparison of particle size distributions of flame C5 case between the present numerical simulation and experimental (Abid *et al.*, 2008) results for different HABs.

Compared with the PSDs of numerical simulation and experimental results, the qualitative agreement can be found. However, the discrepancies of PSDs at lower HAB (i.e., 0.25 and 0.35 cm) flame region cannot be neglected, especially for the PSDs at smaller size regime (i.e., mobility diameter D_p < 4 nm). Such similar large deviations of PSDs also can be found in previous studied numerical simulation results of burner-stabilized stagnation flame (Yapp *et al.*, 2015, Hou *et al.*, 2019). Both Yapp *et al.* (2015)

and Hou *et al.* (2019) also highlighted that such deviation was mainly attributed to two reasons: First was about the nucleation mechanism. Since the fact that the soot nucleation mechanism was still poorly understood and the current nucleation mechanism was rather an approximation. The second was the gas-phase PAH chemistry was still far from reliable. Bakali *et al.* (2012) reported that ABF mechanism overestimate pyrene mole fraction in the sooting region by a significant factor (more than 10) compared with experiments. However, the nucleation rate is very sensitive to the pyrene concentration. In the present study, the deviation of simulated PSDs at smaller particle size regime indicates that the current adopted soot nucleation mechanism is needed further improvement along with more accurate PAH chemistry. On the other hand, the fairly good agreement between numerical simulation and experimental results in PSDs at higher HAB (i.e., HAB$\geqslant$ 0.45 cm) flame region for larger particle size regime (i.e., mobility diameter $D_p \geqslant$ 6 nm) can be found. The PSDs of experimental results are within the range between the PSDs results by imposing the experimental flame temperature profile and solving the energy equation. The relatively good agreement is attributed to coagulation process becomes dominant at higher HAB flame region. The study of different soot dynamic process rates supports this argument as shown in Figure 16. For higher HAB (i.e., HAB$\geqslant$ 0.45 cm), the PSDs finally evolve to distinctly bimodal distribution, and this is clearly captured by our developed LPT-WFMC method, which shows the accuracy of prediction for PSDs from Lagrangian point of view. Since the essential information about soot PSDs is critical for soot prediction. The present numerical simulation results of LPT-WFMC method show that the Lagrangian particle tracking method can be used to capture the full information about the processes of soot formation and evolution.

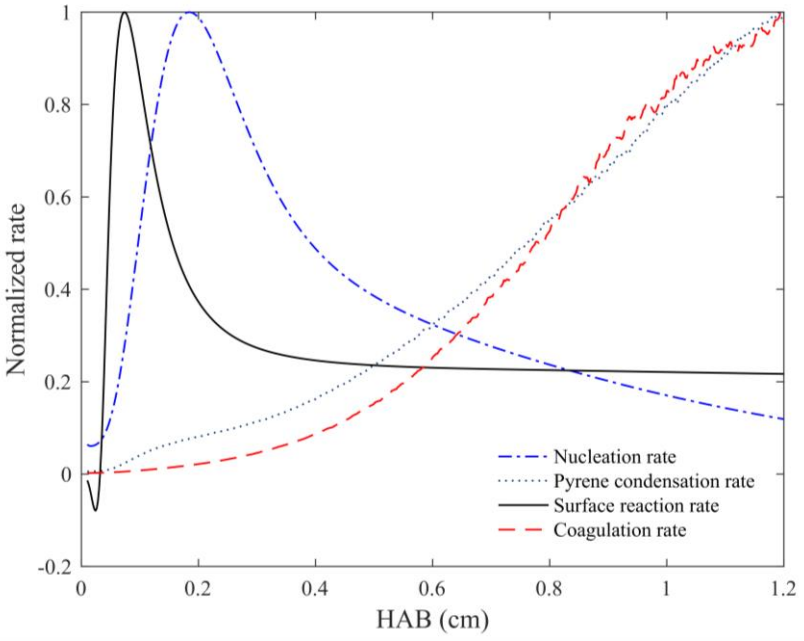

Figure 16 Normalized rate profiles of different soot dynamic processes for different HABs.

In Lagrangian particle tracking approach, the history of individual soot particle can be tracked. In here, flame C3 case is selected to study the rates of different soot dynamic processes as a typical example. Figure 16 shows the rates of nucleation, condensation, surface growth and coagulation for flame C3 case at different HABs. All the rates are normalized by their corresponding maximum values. At lower HAB flame region, nucleation and surface reaction rates dominate the soot dynamic processes and the PSDs is of unimodal distribution (e.g., PSDs at HAB= 0.25 and 0.35 cm). At higher HAB flame region, the nucleation rate decreases significantly because most of particles are formed which lead to condensation and consume more pyrene. Hence, the pyrene concentrations are then decreased as shown in Figure 4. The surface reaction rate is also decreased along with the decreasing of H-atom mole fraction since the rate of surface reaction is proportional to H-atom concentration (Wang, 2011). Although the pyrene condensation rate is increased, but the mass addition by pyrene condensation is relatively small when compared with the surface growth (Veshkini and Dworkin, 2017). Thus, the coagulation process finally dominates PSDs and the PSDs gradually evolves to be of bimodal distribution.

3.4 Parametric sensitivity analysis

Figure 17 schematically shows the typical bimodal PSDs. In order to quantitatively characterize the computed PSDs, the four selected characteristic points on a bimodal PSDs is defined as (Singh *et al.*, 2006, Yapp *et al.*, 2015): (a) the inception peak for nucleation process, (b) a trough for bimodal PSDs, (c) the coagulation peak by coagulation and surface growth processes, (d) the ‘‘largest’’ particle. Here the ‘‘largest’’ particle is defined as the largest diameter with normalized number density of soot particles, $n(D_p) = 10^{-2}$.

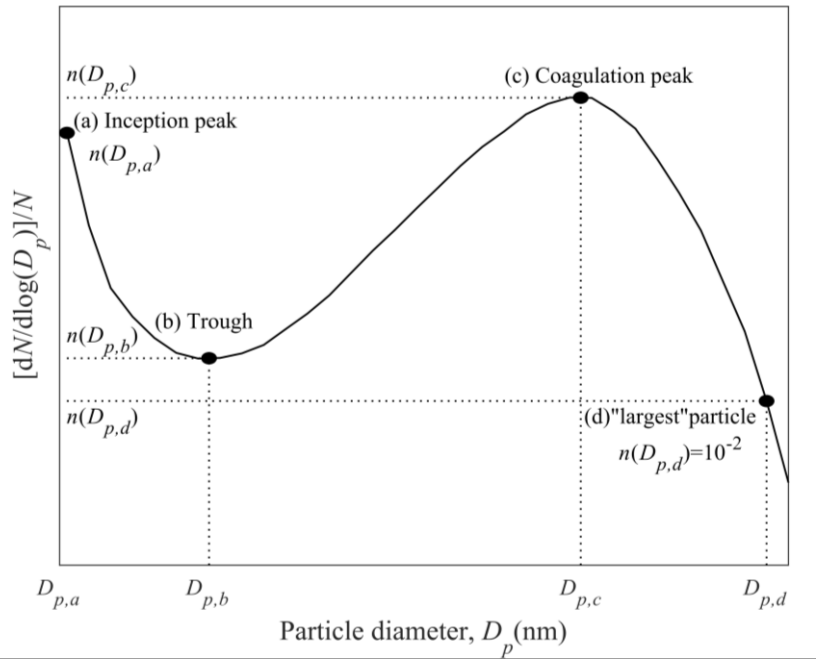

Figure 17 Characteristic particle size distribution function.

In order to study the influence of soot model parameters to the bimodal PSDs, there are some critical parameters taken into the consideration of the parametric sensitivity analysis which include (a) morphology of soot aggregates, (b) density of soot aggregates, (c) pyrene-pyrene sticking probability, (d) the pyrene-particle sticking probability and (e) the particle-particle sticking probability. The parameters ranges and values used for the base cases and references are listed in Table 2.

Table 2 Model parameters for detailed population balance model.

Parameters	Ranges	Value	References
(a) Aggregates morphology	Coalescence to aggregation	VSH model	Blanquart and Pitsch (2009)
(b) Soot density, ρ (g/cm^3)	$0.6 \le \rho \le 2$	1.4	Yapp *et al.* (2015)
(c) pyrene-pyrene sticking probability, $\gamma_{A4\text{-}A4}$	$0 \le \gamma_{A4\text{-}A4} \le 1$	0.025	Blanquart and Pitsch (2009)
(d) pyrene-particle sticking probability, $\gamma_{A4\text{-}P}$	$0 \le \gamma_{A4\text{-}P} \le 1$	0.5	Zhang *et al.* (2009)
(e) particle -particle sticking probability, $\gamma_{P\text{-}P}$	$0 \le \gamma_{P\text{-}P} \le 1$	1	Hou *et al.* (2019)

The flame C3 case is selected as a typical example to illustrate the effect of different parameters on the bimodal PSDs. The numerical simulation is carried out at HAB = 0.85 cm where the PSDs are fully evolved to the bimodal distribution. By varying the studied parameters in Table 2, the parametric sensitivity analysis is applied for the bimodal PSDs. Although many previous sensitivity studies for soot PSDs were conducted (Singh *et al.*, 2006, Yapp *et al.*, 2015, Hou *et al.*, 2019, Hou *et al.*, 2020), the effect of parameters was only qualitatively analyzed. In the present study, the parametric sensitivity of PSDs is quantitatively studied for determining the relative changes in position for some critical points. To quantitatively characterize the parametric sensitivity to the bimodal PSDs, the position changes of characteristic points are defined as

$$S_n = \frac{\log[n(D_p)|_{\text{upper}}] - \log[n(D_p)|_{\text{lower}}]}{\log[n(D_{p,a})|_{\text{base}}] - \log[n(D_{p,d})|_{\text{base}}]} \tag{3.2}$$

$$S_D = \frac{\log[D_p|_{\text{upper}}] - \log[D_p|_{\text{lower}}]}{\log[D_{p,d}|_{\text{base}}] - \log[D_{p,a}|_{\text{base}}]} \tag{3.3}$$

Equations (3.2) and (3.3) are described the relative changes in position of $n(D_p)$ and D_p for the characteristic points. The subscripts of upper and lower mean the values at upper and lower bounds of studied parameters, respectively. The logarithmic value is used here since the PSDs are always studied at logarithm coordinates. If $|S| < 0.1$, the parameter is assumed not sensitive to the position of characteristic point on bimodal PSDs, for $0.1 \leqslant |S| < 0.2$ where the parameter is sensitive**,** and the symbol, $\rightarrow$ is used to denote their change tendency. For $0.2 \leqslant |S|$, the parameter is very sensitive, and the symbol, $\Longrightarrow$ is used to denote their significant change tendency.

For coalescence model, all soot particles are assumed to be spheres, particle will fully coalescence after coagulation events. However, in the aggregation model, each primary particle in soot aggregates is connected only through a point. In the present base case, the joint volume-surface multi-variate (VSH) model is used which between these two limit models. Detailed information about this model can be referred to (Blanquart and Pitsch, 2009).

Figure 18 shows the effects of soot particle coagulation model on bimodal PSDs. The results show the position of trough, coagulation peak and "largest" particles are very sensitive to coagulation model. As coagulation model is adopted from coalescence to aggregation, the trough will drop down, and both coagulation peak and "largest" particles will shift to the larger particle size regime. Since all soot particles are assumed to be spherical particles in coalescence model, but the aggregates are assumed to be a point connected by the primary particle in aggregation model, thus larger mobility diameters are found in aggregation model.

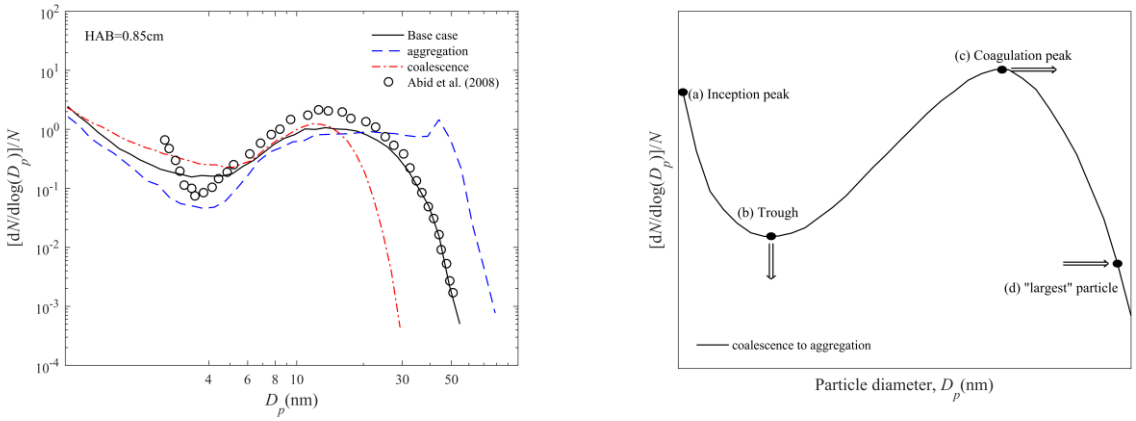

Figure 18 Parametric sensitivity analysis of PSDs for different coagulation models.

Figure 19 shows the parametric sensitivity analysis of soot mass density on bimodal PSDs. The results show only the position of trough are very sensitive to the soot density. As increasing soot mass density, the higher inception peak and trough can be found. Meanwhile, trough, coagulation peak and "largest" particles will shift to the smaller particle size regime. For lower soot mass density, the growth of soot particle sizes is more rapid for given mass growth rate. On the other hand, the coagulation kernel is also the function of particle mass density in free molecular regime. Hence, the smaller soot mass density results in larger coagulation kernel, while the coagulation events occur more frequently which results in more soot particles in larger particle size regime.

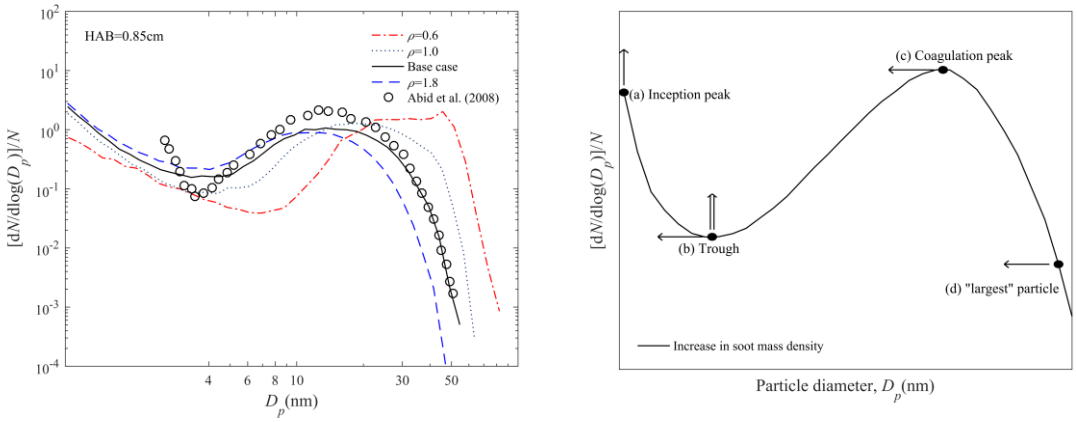

Figure 19 Parametric sensitivity analysis of PSDs for different soot densities.

Figures 20, 21 and 22 show the effects of $\gamma_{A4\text{-}A4}$, $\gamma_{A4\text{-}P}$, and $\gamma_{P\text{-}P}$ on bimodal PSDs, respectively. Increasing $\gamma_{A4\text{-}A4}$ will directly increase the nucleation rate, and results in rising inception peak while decreasing both the trough and coagulation peaks. Besides, the positions of trough, coagulation peak and "largest particle" are systematically shifted to the larger particle size regime. With the increase of $\gamma_{A4\text{-}P}$, the position of "largest particle" nearly maintains unchanged, while the peak positions of coagulation and inception are changed significantly with only a minor shift on the trough. With the decrease of $\gamma_{P\text{-}P}$, it is clearly shown that the trough is vanished at relatively low $\gamma_{P\text{-}P}$ (i.e., $\gamma_{P\text{-}P}$= 0.1 for the present numerical study). As a result, the bimodal PSDs is then evolved to the unimodal PSDs. The inception peak is also decreased dramatically, together with a slightly higher coagulation peak. Both the positions of coagulation peak and "largest particle" will also be shifted to the smaller particle size regime. For the lower of $\gamma_{P\text{-}P}$, the coagulation effect is minor, thus the size of largest particles due to the coagulation events become smaller. The PSDs are then mainly dominated by nucleation and surface growth processes, and become the unimodal PSDs. Overall, the $\gamma_{A4\text{-}A4}$ shows as the most sensitive parameter on bimodal PSDs because of these four selected characteristic points are all very sensitive to $\gamma_{A4\text{-}A4}$.

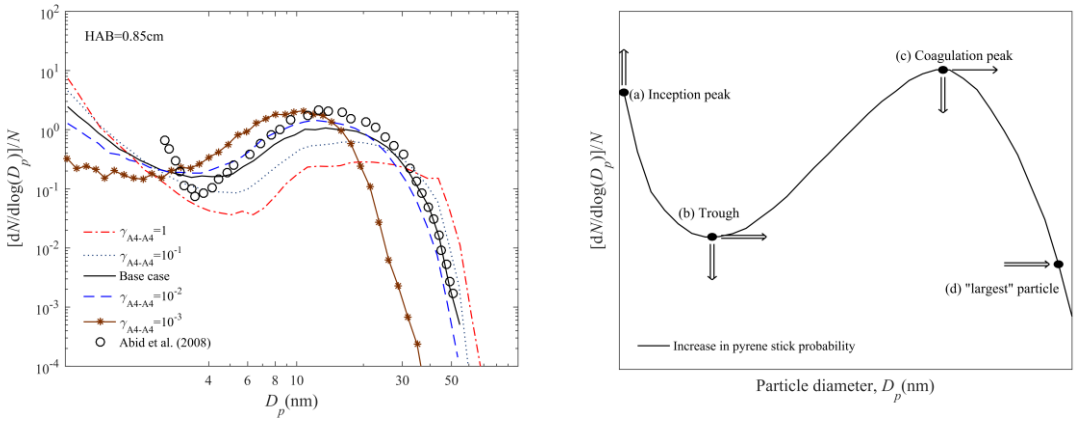

Figure 20 Parametric sensitivity analysis of PSDs for different pyrene-pyrene sticking probabilities.

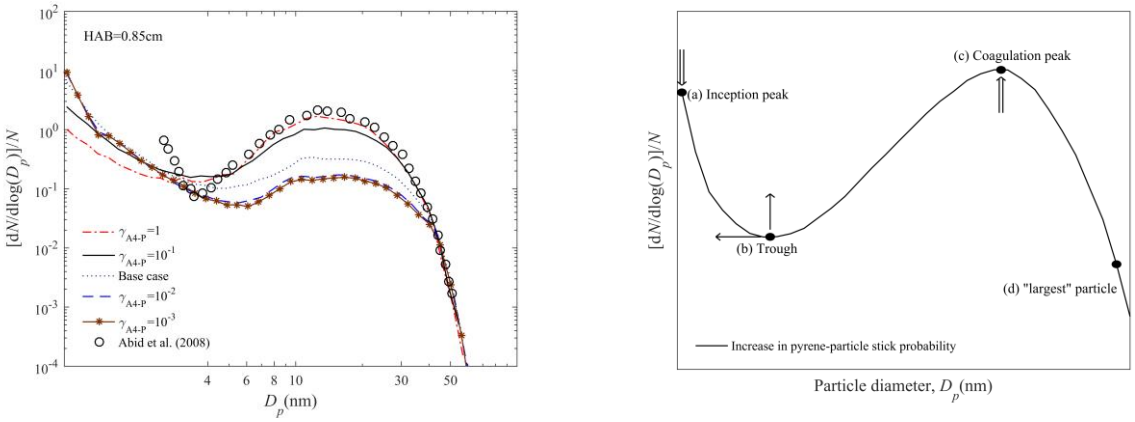

Figure 21 Parametric sensitivity analysis of PSDs for different pyrene-particle sticking probabilities.

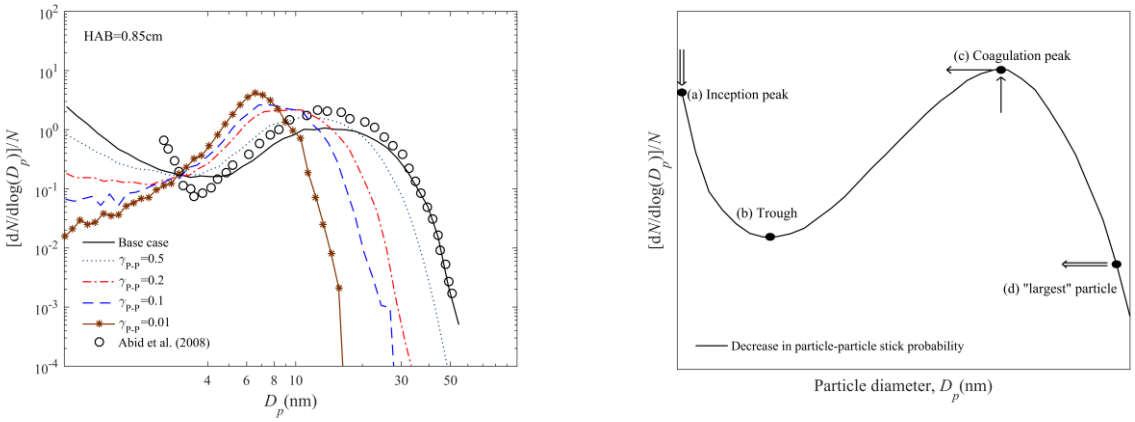

Figure 22 Parametric sensitivity analysis of PSDs for different particle-particle sticking probabilities.

5. Conclusions

Lagrangian particle tracking with a weighted fraction Monte Carlo (LPT-WFMC) method is newly developed and coupled with a detailed soot model to study the soot formation and evolution. The weighted soot particle is used in the MC framework and is tracked using Lagrangian approach. The WFMC method is derived based on the MMC method with adjustable weight distribution by introducing the fraction function α. The LPT-WFMC method is validated for soot prediction in one-dimensional laminar premixed ethylene flame by comparison with the results of DSMC, MMC and the experiments. In the present study, stochastic error analysis has proved that the LPT-WFMC method can extend the soot PSDs and reduce the statistical error for larger particle size regime because LPT-WFMC method can change the numerical weight distribution to assign more particles to larger particle size regime, where are always insufficient number of numerical particles and are the poor represented.

The numerical simulation results for soot number density and volume fraction show the similar trends with experimental results, but still with some overprediction for soot number density as similar to some previous studies. The numerical simulation results of soot PSDs show that a fairly good agreement with experimental results at higher HAB of flame region with larger particle size regime (i.e., HAB$\geqslant$ 0.45cm and D_p> 6 nm). while coagulation and surface growth processes are well captured. However, for lower HAB flame region and smaller particle size regime (i.e., D_p < 4 nm HAB$\leqslant$ 0.35 cm), the large deviations from simulated PSDs and experimental results are not negligible. Such discrepancies for total number density and PSDs at lower HAB flame region and smaller particle size regime indicate that a better understanding and modelling of the soot nucleation and the chemistry of PAHs is still one of the most challenging problems in the research field. The soot PSDs is finally evolved to bimodal distribution which can be explained by studying the rate of soot dynamic process. Parametric sensitivity analysis is also performed to provide a better understanding and gain insight of the effect of those critical parameters on simulated PSDs.

Acknowledgements

This work was supported by the research studentship grant, the General Research Fund, Research Grants Council of the Hong Kong Special Administrative Region, China (Project No. PolyU 152663/16E) and the Central Research Grant (Project No. B-Q54U) and Department of Mechanical Engineering of The Hong Kong Polytechnic University.

References

Abid, A. D., Heinz, N., Tolmachoff, E. D., Phares, D. J., Campbell, C. S. and Wang, H. (2008), "On evolution of particle size distribution functions of incipient soot in premixed ethylene–oxygen–argon flames", *Combustion and Flame,* Vol. 154 No. 4, pp. 775-788.

Allen, M. and Raabe, O. (1982), "Re-evaluation of Millikan's oil drop data for the motion of small particles in air", *Journal of Aerosol Science,* Vol. 13 No. 6, pp. 537-547.

Appel, J., Bockhorn, H. and Frenklach, M. (2000), "Kinetic modeling of soot formation with detailed chemistry and physics: laminar premixed flames of C2 hydrocarbons", *Combustion and flame,* Vol. 121 No. 1-2, pp. 122-136.

Babovsky, H. (1999), "On a Monte Carlo scheme for Smoluchowski's coagulation equation", *Monte Carlo Methods and Applications,* Vol. 5, pp. 1-18.

Blanquart, G. and Pitsch, H. (2009), "A joint volume-surface-hydrogen multi-variate model for soot formation", *Combustion Generated Fine Carbonaceous Particles*, pp. 437-463.

Chan, T. L, Liu, Y. and Chan, C. K. (2010), "Direct quadrature method of moments for the exhaust particle formation and evolution in the wake of the studied ground vehicle", *Journal of Aerosol Science,* Vol. 41 No. 6, pp. 553-568.

Debry, E., Sportisse, B. and Jourdain, B. (2003), "A stochastic approach for the numerical simulation of the general dynamics equation for aerosols", *Journal of Computational Physics,* Vol. 184 No. 2, pp. 649-669.

Dellinger, N., Bertier, N., Dupoirieux, F. and Legros, G. (2020), "Hybrid Eulerian-Lagrangian method for soot modelling applied to ethylene-air premixed flames", *Energy,* Vol. 194, No. 116858.

DeVille, R. E. L., Riemer, N. and West, M. (2011), "Weighted Flow Algorithms (WFA) for stochastic particle coagulation", *Journal of Computational Physics,* Vol. 230 No. 23, pp. 8427-8451.

Eibeck, A. and Wagner, W. (2001), "Stochastic particle approximations for Smoluchoski's coagulation equation", *Annals of Applied Probability*, pp. 1137-1165.

El Bakali, A., Mercier, X., Wartel, M., Acevedo, F., Burns, I., Gasnot, L., Pauwels, J.-F. and Desgroux, P. (2012), "Modeling of PAHs in low pressure sooting premixed methane flame", *Energy,* Vol. 43 No. 1, pp. 73-84.

Fan, J., Zhang, X., Chen, L. and Cen, K. (1997), "New stochastic particle dispersion modeling of a turbulent particle-laden round jet", *Chemical Engineering Journal,* Vol. 66 No. 3, pp. 207-216.

Frenklach, M. (2002), "Method of moments with interpolative closure", *Chemical Engineering Science,* Vol. 57 No. 12, pp. 2229-2239.

Frenklach, M. and Wang, H. (1991), "Detailed modeling of soot particle nucleation and growth", in *Symposium (International) on Combustion*, Vol. 23, pp. 1559-1566.

Frenklach, M. and Wang, H. (1994), "Detailed mechanism and modeling of soot particle formation", *Soot formation in combustion*, Springer pp. 165-192.

Friedlander, S. K. and Smoke, D. (2000), "Smoke, dust, and Haze: Fundamentals of aerosol dynamics", Oxford University Press, New York.

Fuentes, A., Rouvreau, S., Joulain, P., Vantelon, J.-P., Legros, G., Torero, J. L. and Fernandez-Pello, A. (2007), "Sooting behavior dynamics of a non-buoyant laminar diffusion flame", *Combustion science and technology,* Vol. 179 No. 1-2, pp. 3-19.

Gallen, L., Felden, A., Riber, E. and Cuenot, B. (2019), "Lagrangian tracking of soot particles in LES of gas turbines", *Proceedings of the Combustion Institute,* Vol. 37 No. 4, pp. 5429-5436.

Gelbard, F., Tambour, Y. and Seinfeld, J. H. (1980), "Sectional representations for simulating aerosol dynamics", *Journal of Colloid and Interface Science,* Vol. 76 No. 2, pp. 541-556.

Hoerlle, C. A., França, F. H. R., Pagot, P. R. and Pereira, F. M. (2020), "Effects of radiation modeling on non-premixed sooting flames simulations under oxyfuel conditions", *Combustion and Flame*, Vol. 217, pp. 294-305.

Hou, D., Lindberg, C. S., Manuputty, M. Y., You, X. and Kraft, M. (2019), "Modelling soot formation in a benchmark ethylene stagnation flame with a new detailed population balance model", *Combustion and Flame,* Vol. 203, pp. 56-71.

Hou, D., Lindberg, C. S., Wang, M., Manuputty, M. Y., You, X. and Kraft, M. (2020), "Simulation of primary particle size distributions in a premixed ethylene stagnation flame", *Combustion and Flame,* Vol. 216, pp. 126-135.

Issa, R. I. (1986), "Solution of the implicitly discretised fluid flow equations by operator-splitting", *Journal of Computational Physics,* Vol. 62 No. 1, pp. 40-65.

Jasak, H., Jemcov, A. and Tukovic, Z. (2007), "OpenFOAM: A C++ library for complex physics simulations", in *International workshop on coupled methods in numerical dynamics*, Zagreb, Croatia, 19-21 September 2007, pp. 47-66.

Jiang, X. and Chan, T. L. (2021), "A new weighted fraction Monte Carlo method for particle coagulation", *International Journal of Numerical Methods for Heat & Fluid Flow*, Early access: Feb. 2021.

Katta, V. R., Blevins, L. G. and Roquemore, W. M. (2005), "Dynamics of an inverse diffusion flame and its role in polycyclic-aromatic-hydrocarbon and soot formation", *Combustion and Flame,* Vol. 142 No. 1-2, pp. 33-51.

Kazakov, A. and Foster, D. E. (1998), "Modeling of soot formation during DI diesel combustion using a multi-step phenomenological model", *SAE transactions*, pp. 1016-1028.

Kazakov, A., Wang, H. and Frenklach, M. (1995), "Detailed modeling of soot formation in laminar premixed ethylene flames at a pressure of 10 bar", *Combustion and Flame,* Vol. 100 No. 1-2, pp. 111-120.

Kee, R. J., Grcar, J. F., Smooke, M. D., Miller, J. A. and Meeks, E. (1985), "PREMIX: a Fortran program for modeling steady laminar one-dimensional premixed flames", *Sandia National Laboratories Report,* No. SAND85-8249.

Kennedy, I. M. (1997), "Models of soot formation and oxidation", *Progress in Energy and Combustion Science,* Vol. 23 No. 2, pp. 95-132.

Kholghy, M. R. and Kelesidis, G. A. (2021), "Surface growth, coagulation and oxidation of soot by a monodisperse population balance model", *Combustion and Flame*, Vol. 227, pp. 456-463.

Kotalczyk, G. and Kruis, F. E. (2017), "A Monte Carlo method for the simulation of coagulation and nucleation based on weighted particles and the concepts of stochastic resolution and merging", *Journal of Computational Physics,* Vol. 340, pp. 276-296.

Kraft, M. (2005), "Modelling of particulate processes", *KONA Powder and Particle Journal,* Vol. 23, pp. 18-35.

Kronholm, D. F. and Howard, J. B. (2000), "Analysis of soot surface growth pathways using published plug-flow reactor data with new particle size distribution measurements and published premixed flame data", *Proceedings of the Combustion Institute,* Vol. 28 No. 2, pp. 2555-2561.

Kruis, F. E., Maisels, A. and Fissan, H. (2000), "Direct simulation Monte Carlo method for particle coagulation and aggregation", *AIChE Journal,* Vol. 46 No. 9, pp. 1735-1742.

Kumfer, B. and Kennedy, I. (2009), "The role of soot in the health effects of inhaled airborne particles", in *Combustion generated fine carbonaceous particles, Proceedings of an international workshop held in Villa Orlandi, Anacapri, May 13, 2007, KIT Scientific Publishing*, pp. 1-15.

Kuo, K. K. (2005), *Principles of combustion,* Hoboken, New Jersey : John Wiley

Liffman, K. (1992), "A direct simulation Monte-Carlo method for cluster coagulation", *Journal of Computational Physics,* Vol. 100 No. 1, pp. 116-127.

Liu, H. M. and Chan, T. L. (2018a), "Differentially weighted operator splitting Monte Carlo method for simulating complex aerosol dynamic processes", *Particuology,* Vol. 36, pp. 114-126.

Liu, H. M. and Chan, T. L. (2019), "A coupled LES-Monte Carlo method for simulating aerosol dynamics in a turbulent planar jet", *International Journal of Numerical Methods for Heat & Fluid Flow*.

Liu, H. M. and Chan, T. L. (2018b), "Two-component aerosol dynamic simulation using differentially weighted operator splitting Monte Carlo method", *Applied Mathematical Modelling,* Vol. 62, pp. 237-253.

Liu, S. Y. and Chan, T. L. (2017), "A stochastically weighted operator splitting Monte Carlo (SWOSMC) method for the numerical simulation of complex aerosol dynamic processes", *International Journal of Numerical Methods for Heat & Fluid Flow*.

Liu, S. Y., Chan, T. L., He, Z., Lu, Y., Jiang, X. and Wei, F. (2019a), "Soot formation and evolution characteristics in premixed methane/ethylene-oxygen-argon burner-stabilized stagnation flames", *Fuel,* Vol. 242, pp. 871-882.

Liu, S. Y., Chan, T. L., Lin, J. Z.. and Yu, M. Z. (2019b), "Numerical study on fractal-like soot aggregate dynamics of turbulent ethylene-oxygen flame", *Fuel,* Vol. 256, p. 115857.

Liu, Y. H., He, Z. and Chan, T. L. (2011), "Three-dimensional simulation of exhaust particle dispersion and concentration fields in the near-wake region of the studied ground vehicle", *Aerosol science and technology,* Vol. 45 No. 8, pp. 1019-1030.

Marchisio, D. L. and Fox, R. O. (2013), *Computational models for polydisperse particulate and multiphase systems,* Cambridge University Press, .

Menz, W. J. and Kraft, M. (2013), "A new model for silicon nanoparticle synthesis", *Combustion and flame,* Vol. 160 No. 5, pp. 947-958.

Menz, W. J., Patterson, R. I., Wagner, W. and Kraft, M. (2013), "Application of stochastic weighted algorithms to a multidimensional silica particle model", *Journal of Computational Physics,* Vol. 248, pp. 221-234.

Micklow, G. and Gong, W. (2002), "A multistage combustion model and soot formation model for direct-injection diesel engines", *Proceedings of the Institution of Mechanical Engineers, Part D: Journal of Automobile Engineering,* Vol. 216 No. 6, pp. 495-504.

Mueller, M. E., Blanquart, G. and Pitsch, H. (2009), "A joint volume-surface model of soot aggregation with the method of moments", *Proceedings of the Combustion Institute,* Vol. 32 No. 1, pp. 785-792.

Neoh, K., Howard, J. and Sarofim, A. (1981), "Soot oxidation in flames", *Particulate Carbon*, Springer, pp. 261-282.

Ong, J. C., Pang, K. M., Walther, J. H., Ho, J.-H. and Ng, H. K. (2018), "Evaluation of a Lagrangian Soot Tracking Method for the prediction of primary soot particle size under engine-like conditions", *Journal of Aerosol Science,* Vol. 115, pp. 70-95.

OpenCFD (2019), "OpenCFD Release OpenFOAM", https://www.openfoam.com/releases/openfoam-v1906.

Park, S., Rogak, S., Bushe, W., Wen, J. and Thomson, M. (2005), "An aerosol model to predict size and structure of soot particles", *Combustion Theory and Modelling,* Vol. 9 No. 3, pp. 499-513.

Patterson, R. I., Wagner, W. and Kraft, M. (2011), "Stochastic weighted particle methods for population balance equations", *Journal of Computational Physics,* Vol. 230 No. 19, pp. 7456-7472.

Prakash, A., Bapat, A. and Zachariah, M. (2003), "A simple numerical algorithm and software for solution of nucleation, surface growth, and coagulation problems", *Aerosol Science & Technology,* Vol. 37 No. 11, pp. 892-898.

Qiu, L., Hua, Y., Cheng, X., Zhuang, Y. and Qian, Y. (2019), "Numerical investigation of soot formation in a methane diffusion flame doped with n-heptane at elevated pressure", *Energy & Fuels*, Vol. 33 No. 11, pp. 11941-11947.

Rigopoulos, S. (2010), "Population balance modelling of polydispersed particles in reactive flows", *Progress in Energy and Combustion Science,* Vol. 36 No. 4, pp. 412-443.

Saggese, C., Cuoci, A., Frassoldati, A., Ferrario, S., Camacho, J., Wang, H. and Faravelli, T. (2016), "Probe effects in soot sampling from a burner-stabilized stagnation flame", *Combustion and Flame,* Vol. 167, pp. 184-197.

Saggese, C., Ferrario, S., Camacho, J., Cuoci, A., Frassoldati, A., Ranzi, E., Wang, H. and Faravelli, T. (2015), "Kinetic modeling of particle size distribution of soot in a premixed burner-stabilized stagnation ethylene flame", *Combustion and Flame*, Vol. 162 No. 9, pp. 3356-3369.

Salenbauch, S., Cuoci, A., Frassoldati, A., Saggese, C., Faravelli, T. and Hasse, C. (2015), "Modeling soot formation in premixed flames using an extended conditional quadrature method of moments", *Combustion and Flame,* Vol. 162 No. 6, pp. 2529-2543.

Selvaraj, P., Arias, P. G., Lee, B. J., Im, H. G., Wang, Y., Gao, Y., Park, S., Sarathy, S. M., Lu, T. and Chung, S. H. (2016), "A computational study of ethylene–air sooting flames: Effects of large polycyclic aromatic hydrocarbons", *Combustion and Flame*, Vol. 163, pp. 427-436.

Singh, J., Patterson, R. I., Kraft, M. and Wang, H. (2006), "Numerical simulation and sensitivity analysis of detailed soot particle size distribution in laminar premixed ethylene flames", *Combustion and Flame,* Vol. 145 No. 1-2, pp. 117-127.

Smith, M. and Matsoukas, T. (1998), "Constant-number Monte Carlo simulation of population balances", *Chemical Engineering Science,* Vol. 53 No. 9, pp. 1777-1786.

Smoluchowski, M. v. (1916), "Drei vortrage uber diffusion, brownsche bewegung und koagulation von kolloidteilchen", *ZPhy,* Vol. 17, pp. 557-585.

Song, Y. N. and Zhong, B. J. (2008), "Modeling of soot and polycyclic aromatic hydrocarbons in diesel diffusion combustion", *Chemical Engineering & Technology,* Vol. 31 No. 10, pp. 1418-1423.

Tang, Q., Cai, R., You, X. and Jiang, J. (2017), "Nascent soot particle size distributions down to 1 nm from a laminar premixed burner-stabilized stagnation ethylene flame", *Proceedings of the Combustion Institute,* Vol. 36 No. 1, pp. 993-1000.

Thajudeen, T., Jeon, S. and Hogan Jr, C. J. (2015), "The mobilities of flame synthesized aggregates/agglomerates in the transition regime", *Journal of Aerosol Science*, Vol. 80, pp. 45-57.

Tian, L., Schiener, M. and Lindstedt, R. (2020), "Fully coupled sectional modelling of soot particle dynamics in a turbulent diffusion flame", *Proceedings of the Combustion Institute*, Vol. 38 No. 1, pp. 1365-1373.

Veshkini, A. and Dworkin, S. B. (2017), "A computational study of soot formation and flame structure of coflow laminar methane/air diffusion flames under microgravity and normal gravity", *Combustion Theory and Modelling,* Vol. 21 No. 5, pp. 864-878.

Waldmann, L. (1961), "On the motion of spherical pariticles in nonhomogeneous gases", *Rarefied gas dynamics*.

Wang, B., Mosbach, S., Schmutzhard, S., Shuai, S., Huang, Y. and Kraft, M. (2016), "Modelling soot formation from wall films in a gasoline direct injection engine using a detailed population balance model", *Applied Energy,* Vol. 163, pp. 154-166.

Wang, H. (2011), "Formation of nascent soot and other condensed-phase materials in flames", *Proceedings of the Combustion Institute,* Vol. 33 No. 1, pp. 41-67.

Wen, J. Z., Thomson, M., Park, S., Rogak, S. and Lightstone, M. (2005), "Study of soot growth in a plug flow reactor using a moving sectional model", *Proceedings of the Combustion Institute*, Vol. 30 No. 1, pp. 1477-1484.

Wu, S., Yang, W., Xu, H. and Jiang, Y. (2019), "Investigation of soot aggregate formation and oxidation in compression ignition engines with a pseudo bi-variate soot model", *Applied Energy,* Vol. 253, No. 113609.

Xu, Z., Zhao, H. and Zheng, C. (2015), "Accelerating population balance-Monte Carlo simulation for coagulation dynamics from the Markov jump model, stochastic algorithm and GPU parallel computing", *Journal of Computational Physics,* Vol. 281, pp. 844-863.

Yang, S. and Mueller, M. E. (2019), "A Multi-Moment Sectional Method (MMSM) for tracking the soot Number Density Function", *Proceedings of the Combustion Institute,* Vol. 37 No. 1, pp. 1041-1048.

Yapp, E. K., Chen, D., Akroyd, J., Mosbach, S., Kraft, M., Camacho, J. and Wang, H. (2015), "Numerical simulation and parametric sensitivity study of particle size distributions in a burner-stabilised stagnation flame", *Combustion and Flame,* Vol. 162 No. 6, pp. 2569-2581.

Yu, M. Z., Lin, J. Z., Seipenbusch, M. and Cao, J. (2017), "Verification of size-resolved population balance modeling for engineered nanoparticles under high concentration", *Chemical Engineering Journal*, Vol. 323, pp. 592-604.

Yu, M. Z., Lin, J. Z. and Chan, T. L. (2008), "A new moment method for solving the coagulation equation for particles in Brownian motion", *Aerosol Science and Technology,* Vol. 42 No. 9, pp. 705-713.

Zhang, Q., Guo, H., Liu, F., Smallwood, G. and Thomson, M. (2009), "Modeling of soot aggregate formation and size distribution in a laminar ethylene/air coflow diffusion flame with detailed PAH chemistry and an advanced sectional aerosol dynamics model", *Proceedings of the Combustion Institute,* Vol. 32 No. 1, pp. 761-768.

Zhao, H., Kruis, F. E. and Zheng, C. (2009), "Reducing statistical noise and extending the size spectrum by applying weighted simulation particles in Monte Carlo simulation of coagulation", *Aerosol Science and Technology,* Vol. 43 No. 8, pp. 781-793.

Zhou, K., Jiang, X. and Chan, T. L. (2020), "Error analysis in stochastic solutions of population balance equations", *Applied Mathematical Modelling,* Vol. 80, pp. 531-552.

Zhou, K., He, Z., Xiao, M. and Zhang, Z. (2014), "Parallel Monte Carlo simulation of aerosol dynamics", *Advances in Mechanical Engineering,* Vol. 6, No. 435936.

Zhu, H., Zhou, Z., Yang, R. and Yu, A. (2007), "Discrete particle simulation of particulate systems: theoretical developments", *Chemical Engineering Science,* Vol. 62 No. 13, pp. 3378-3396.